FERMILAB-Pub-89/239-A
CfPA-TH-89-016
Nov 1989

Supersymmetric Dark Matter Above the W Mass

KIM GRIEST,[1] MARC KAMIONKOWSKI,[2,3] AND MICHAEL S. TURNER[2,3]

[1] *Center for Particle Astrophysics, University of California, Berkeley, CA 94720*

[2] *Department of Physics and Enrico Fermi Institute, The University of Chicago, Chicago, IL 60637-1433*

[3] *NASA/Fermilab Astrophysics Center, Fermi National Accelerator Laboratory, Batavia, IL 60510-0500*

ABSTRACT

In this paper we study the cosmological consequences of the minimal supersymmetric extension of the standard model in the case that the neutralino is heavier than the W. We calculate the cross section for annihilation of heavy neutralinos into final states containing gauge and Higgs bosons ($\widetilde{\chi}\widetilde{\chi} \to WW$, ZZ, HH, HW, HZ) and combine these results with those previously obtained for annihilation into fermions to find the relic cosmological abundance for the most general neutralino. The new channels are particularly important for Higgsino-like and mixed-state neutralinos, but are sub-dominant (to the fermion-antifermion annihilation channels) in the case that the neutralino is mostly a gaugino. The effect of the top quark mass is also considered. Using these cross sections and the cosmological constraint $\Omega_{\tilde{\chi}} h^2 \lesssim 1$, we map the entire range of cosmologically acceptable supersymmetric parameter space and discover a very general bound on the neutralino mass. For a top quark mass of less than 180 GeV, neutralinos heavier than 3200 GeV are cosmologically inconsistent, and if the top quark mass is less than 120 GeV, the bound is lowered to 2600 GeV. Neutralino states that are mostly gaugino are constrained to be lighter than 550 GeV. We find that a "heavy" neutralino ($m_{\tilde{\chi}} > m_W$) that contributes $\Omega_{\tilde{\chi}} \sim 1$ arises for a very wide range of model parameters and makes, therefore, a very natural and attractive dark matter candidate.

I. INTRODUCTION

Low-energy-supersymmetric theories provide an elegant solution to the hierarchy problem and have been extensively studied in recent years.[1] In most models, the lightest supersymmetric particle (LSP) is stable and makes an attractive candidate for the dark matter known to exist throughout the Universe and especially that in galactic halos.[2,3] In the minimal supersymmetric model, the most likely LSP is the neutralino—a linear combination of photino, Higgsino, and Z-ino fields. In addition, it has been shown that if it exists and is stable, it very naturally has a relic abundance near closure density, and thus probably comprises a significant component of our galactic halo independent of the parameters of the supersymmetric model.[4,5] However, in previous work it has been implicitly assumed that the mass of the neutralino, $m_{\tilde{\chi}}$, is less than the W mass. (But see the recent work of Olive and Srednicki.[6]) Important new annihilation channels open up when $m_{\tilde{\chi}} > m_W$ and because the relic abundance is determined by the total annihilation cross section, it is crucial to include these new channels. In particular, the results of Refs. 4 and 5 were found considering only the reaction $\tilde{\chi}\tilde{\chi} \to f\bar{f}$, where f is a quark or lepton, while for $m_{\tilde{\chi}} > m_W$ final states such as W^+W^-, ZZ, and states involving Higgs bosons must also be included. For Dirac neutrino dark matter, it was shown by Enqvist, Kainulainen, and Maalampi[7] that the gauge-boson final states dominate as the neutrino mass increases, and we show that the same is true for the neutralino in some regions of supersymmetric parameter space.

Since a supersymmetric solution to the hierarchy problem requires a relatively light LSP, an "extremely" massive neutralino is not very attractive;[8] however, masses in the 100 GeV range are entirely reasonable, especially as unsuccessful accelerator searches push the possible masses of the supersymmetric particles upward. In this paper, we consider in detail the possibility of neutralino dark matter heavier than the W, *i.e.*, $m_{\tilde{\chi}} \gtrsim m_W$. Regions of parameter space that are ruled out due to an excessive relic density of neutralinos are identified and the cosmologically viable range of neutralino masses is found to be in a range

that is also suitable for solving the naturalness problem. We also show that the cosmologically acceptable supersymmetric models naturally predict relic abundances in the range appropriate for supplying the bulk of the dark matter. We find both of these results encouraging.

The plan of this paper is as follows: In Section II, we describe the low-energy-supersymmetric model upon which our calculations are based and describe the calculation of the relevant annihilation cross sections. The complete calculation is done for the W^+W^-, ZZ, and neutral Higgs final states, and reasonable estimates are made for the charged Higgs and mixed Higgs-gauge–boson final states. We then compare the cross sections for these channels to those previously computed for the fermion-antifermion final states and map out the regions of supersymmetric parameter space where the new channels are dominant and the regions where they can safely be ignored. In Section III, we identify those regions of M-μ space that are ruled out by cosmological considerations and obtain a maximum mass for a cosmologically viable neutralino. In Section IV, the remaining cosmologically acceptable regions of parameter space are mapped out and it is shown that for most models, an interesting relic abundance ($0.01 \lesssim \Omega_{\tilde{\chi}} \lesssim 1$) is possible, if not probable. Section V is a summary of the paper and the four Appendixes contain the detailed expressions for the cross sections as well as their forms in several useful limiting cases.

II. MODEL AND CROSS SECTIONS

We start with the minimal supersymmetric extension of the standard model as described by Haber and Kane[1] and follow their conventions and notation throughout. In these models there are four neutralinos, linear combinations of the partners of the photon, Z, and two neutral Higgs bosons; we refer to the lightest (the n^{th} neutralino) as *the* neutralino and denote it as $\tilde{\chi}$,

$$\tilde{\chi} = Z_{n1}\tilde{B} + Z_{n2}\tilde{W}^3 + Z_{n3}\tilde{H}_1 + Z_{n4}\tilde{H}_2, \tag{1}$$

where $(Z)_{ij}$ is the real orthogonal matrix that diagonalizes the neutralino mass matrix. In addition, there are two charginos, linear combinations of the partners of the charged Higgs and gauge bosons. The neutralino and chargino masses and

mixings are determined by three[10] arbitrary parameters: two mass parameters, μ and M, and the ratio of Higgs vacuum expectation values, $\tan\beta = v_2/v_1$. In addition, there are scalar quarks and scalar leptons whose masses are arbitrary, but to simplify matters, a single common squark and slepton mass $m_{\tilde{f}}$, is assumed. Finally, there are the two requisite Higgs doublets which give rise to two neutral scalars H_1^0 and H_2^0, a neutral pseudoscalar H_3^0, and two charged Higgs bosons, H^+ and H^-. The masses and couplings of these particles are determined by μ, M, and $\tan\beta$, as well as the mass of the lightest scalar $m_{H_2^0}$ (see Refs. 11 and 12). In these models the masses of the neutral Higgs particles satisfy: $m_{H_1^0} > m_Z$; $m_{H_2^0} < m_Z \cos 2\beta$; and $m_{H_2^0} < m_{H_3^0} < m_{H_1^0}$. The charged Higgs particles are both heavier than the W. Feynman rules as well as mass matrices and other relevant formulas for the Higgs particles can be found in Refs. 11 and 12.

Although the analysis of the heavy neutralino can become very involved, many results can be understood in terms of the neutralino properties displayed in Fig. 1. The broken curves in Fig. 1 are neutralino mass contours in the M-μ plane, and the solid curves are the gaugino fraction (defined as $Z_{n1}^2 + Z_{n2}^2$) of the neutralino. In Fig. 1, $\tan\beta = 2$ is assumed; however, these curves are relatively insensitive to the value of $\tan\beta$. The mass contours are hyperbolas that asymptote to $m_{\tilde{\chi}} = |\mu|$ for large M and to $m_{\tilde{\chi}} = M' \approx M/2$ for large $|\mu|$. For large values of $|\mu|$ and M, models where the neutralino is half Higgsino and half gaugino fall along the line $\mu = \frac{5}{3} M \tan^2\theta_W \approx M/2$. In the regions where the gaugino fraction is greater than 0.99, $\tilde{\chi}$ is almost a pure B-ino state ($Z_{n1} \approx 1$ and $Z_{ni} \approx 0$ for $i \neq 1$). (When $M' = \frac{5}{3} M \tan^2\theta_W$, the lightest neutralino cannot both be a pure photino and heavier than the W.) When the gaugino fraction is less than 0.01, $\tilde{\chi}$ is very nearly a pure Higgsino state ($Z_{n1} \approx Z_{n2} \approx 0$).

In order to calculate the relic abundance we need the total cross section for annihilation of neutralinos into all lighter particles. The result for $f\bar{f}$ final states, where f is a quark or lepton, has been calculated previously[5] and appears (with corrections) in Appendix D. Other possible final states include the gauge bosons, W^+W^- and ZZ, the six possible combinations of two neutral Higgs bosons ($H_1^0 H_1^0$, $H_1^0 H_2^0$, $H_2^0 H_3^0$, etc.), the charged Higgs, H^+H^-, and the five

Higgs-gauge-boson final states, W^+H^-, W^-H^+, ZH_1^o, ZH_2^o, and ZH_3^o.

Consider the gauge-boson final states first. The Feynman diagrams for $\widetilde{\chi}\widetilde{\chi} \to W^+W^-$ are shown in Fig. 2, and the diagrams for $\widetilde{\chi}\widetilde{\chi} \to ZZ$ are shown in Fig. 3. There are a total of seven diagrams contributing to the WW final state and ten to the ZZ final state. The complete cross sections are given in Appendixes A and B. The calculation of these cross sections is a tedious process with ample opportunity for error; moreover, the final expressions for the cross sections are long. Fortunately, unitarity provides a very nice check. The contributions of the individual Feynman diagrams in Fig. 2 to the cross section for annihilation into W^+W^- contain terms proportional to s, the center of mass energy squared. However, each partial wave of the *complete* matrix element must be bounded by a constant which implies that as $s \to \infty$, the total cross section must be proportional to s^{-1}. For this to occur, a highly nontrivial cancellation must take place between the squares of the seven individual diagrams and the twenty-one interference terms. The formulas for the total cross section presented in Appendix A (as well as those for the ZZ final state presented in Appendix B) do indeed exhibit this behavior. In addition, in the low-energy limit, relative velocity $v \to 0$, the total cross sections reduce to simple squares, Eqs. (A10) and (B7). The correct high-energy behavior of the total cross sections as well as the fact that the cross sections simplify in the $v \to 0$ limit give us some confidence that our complicated expressions are correct.

The Feynman diagrams for $\widetilde{\chi}\widetilde{\chi} \to H_i^0 H_j^0$ are shown in Figs. 4 and 5, and the resulting cross sections are given in Appendix C. None of the squares of the individual diagrams for these channels diverge for large s, so unitarity cannot be used to check our results. Moreover, there is no particular use in obtaining expressions that are exact in s. Therefore, we have obtained expressions that are correct only to order v^2, which simplifies matters greatly. The Higgs-boson channels tend to be sub-dominant to the gauge-boson and fermion-antifermion channels for most of the heavy neutralino parameter space; however, some of the $H_i^0 H_j^0$ final states are quite important when $m_{\tilde{\chi}} < m_W$ and the effect of Higgs-boson final states on light neutralinos is considered in another paper.[9] As

a check, a symbolic manipulation program (MACSYMA) was also used to derive these cross sections and numerical agreement between the MACSYMA results and the formulas of Appendix C was found.

We have completed preliminary calculations for the mixed Higgs-gauge–boson final states, but do not include those results here because these channels seem to be sub-dominant. Since the matrix elements for these channels contain couplings that appear in the pure-Higgs or gauge-boson final states, the cross sections for the mixed channels should lie in between those for the Higgs-boson final states and those for gauge-boson final states. Since the cross sections for the Higgs-boson final states and those for the gauge-boson final states are rarely of the same magnitude for heavy neutralinos, the mixed states should be negligible. Numerically, our preliminary results support this hypothesis.

To see the importance of the bosonic final states, we compare the newly calculated cross sections with the previously calculated annihilation cross section ($\bar{f}f$ final states only).[5] Unfortunately, even with the simplifications already made, a six-dimensional parameter space (μ, M, $\tan\beta$, $m_{H_2^0}$, $m_{\tilde{f}}$, and the top quark mass, m_t) must be explored. To simplify matters we consider only three values of $m_{\tilde{f}}$: $m_{\tilde{f}} = m_{\tilde{\chi}}$, $m_{\tilde{f}} = 2m_{\tilde{\chi}}$, and $m_{\tilde{f}} = \infty$. Recall that $m_{\tilde{\chi}}$ provides a *lower* limit to the squark mass since $\tilde{\chi}$ is assumed to be the LSP. When using $m_{\tilde{f}} = m_{\tilde{\chi}}$, the importance of the new (bosonic) final states will be *underestimated* because $m_{\tilde{f}}$ appears only in the denominator of the cross section into $\bar{f}f$. The opposite limit, $m_{\tilde{f}} = \infty$, supresses the fermion channels greatly, so by considering both limits the sensitivity of our results on $m_{\tilde{f}}/m_{\tilde{\chi}}$ can be seen.

To simplify further, we will set $m_{H_2^0} = 0$. The lightest Higgs mass $m_{H_2^0}$ determines a Higgs mixing angle α, and coupling constants of the Higgs bosons depend only trigonometrically on α. When annihilation into all bosonic final states is considered, the total cross section is relatively insensitive to the choice of $m_{H_2^0}$ provided that the neutralino is heavy enough that threshold effects are unimportant. (As discussed in Ref. 9, the value of $m_{H_2^0}$ is important for light neutralinos.) For the cases presented below, we have confirmed numerically that the results are insensitive to value of $m_{H_2^0}$. We have included Higgs exchange in

the fermion channels, but for very massive neutralinos this effect is not important. As discussed in Ref. 9, Higgs exchange can be important, but only when near a pole.

Using $m_{\tilde{f}} = m_{\tilde{\chi}}$ and $m_{H_2^0} = 0$, we show in Fig. 6 the regions of the M-μ plane where the new final states are important for several values of $\tan\beta$ and m_t and for a neutralino-neutralino relative velocity of $v^2 \approx 1/4$ (relevant for annihilation in the early Universe around "freeze-out"). In the regions "hatched" with positively sloped lines, the annihilation cross section into fermion final states is greater than that into gauge and Higgs bosons by at least a factor of ten. In the areas hatched with negatively sloped lines, the gauge-boson contribution to the annihilation cross section is at least ten times as great as that of the Higgs and fermion channels, and in the regions hatched with horizontal lines, the Higgs-boson contribution dominates that of fermions and gauge bosons by at least a factor of ten. In the areas hatched with vertical lines, none of the three contributions dominate by more than a factor of ten.

The analogous plots for a relative velocity $v^2 \approx 0$ are very similar and so are not shown. We remind the reader that there are two distinct energy regimes of interest for $\widetilde{\chi}\widetilde{\chi}$ annihilation: $v^2 \approx 1/4$, typical of the early Universe around "freeze-out" when the annihilation cross section determines the relic abundance of neutralinos; and $v^2 \approx 10^{-6} \approx 0$, characteristic of the neutralino annihilations in the galactic halo or in the body of the Sun or Earth, which may prove to be an interesting source for high-energy cosmic rays or neutrinos. Since the relative velocity is small in both regimes, an expansion to first order in powers of v^2 is a good approximation for the total annihilation cross section σv. In the early Universe, one might expect the v^2 term in σv to be smaller by a factor of $v^2/4 \approx 1/16$, but for Majorana particles such as the neutralino, the v^0 term may be suppressed and the v^2 term may actually dominate.[13] For present day annihilations with $v^2/4 < 10^{-6}$, the v^2 term in the cross section is never important. Even if the v^0 term vanished at tree level, one would expect higher-order corrections and/or three-body final states to overwhelm the v^2 term in this velocity regime.[14] Given the different possible structures of the cross section in the two velocity regimes, it may be surprising that the figure corresponding to Fig. 6

with $v = 0$ (not shown) looks so similar. In regions of large neutralino mass this similarity occurs because the cross section for annihilation into gauge bosons and top quarks has no s-wave (v^0 term) suppression. In the regions of small $m_{\tilde{\chi}}$, the similarity is due to our assumption that $m_{H_2^0} = 0$. The $H_2^0 H_3^0$ channel in particular is always open and has no s-wave suppression. If we use larger (and more realistic) values for $m_{H_2^0}$ so that annihilation of light neutralinos into Higgs bosons is kinematically forbidden, the behavior of the total annihilation cross section in the galactic halo differs from that in the early Universe. We address this further in Ref. 9.

From Fig. 6 we see that the gauge-boson final states dominate the annihilation cross section when μ is small which corresponds to a "Higgsino-like" neutralino state. In this case, $Z_{n1} \approx Z_{n2} \approx 0$ and $|Z_{n3}| \approx |Z_{n4}| \approx 1/\sqrt{2}$, and the annihilation into W^+W^- (ZZ) proceeds through the t- and u-channel exchange of the lightest chargino (neutralino) with couplings that only depend weakly upon $\tan\beta$. For $m_{\tilde{f}} = m_{\tilde{\chi}}$, annihilation into fermions proceeds mainly through t- and u-channel exchange of the squark, and from the form of the couplings in Appendix D, we see that annihilation into the $b\bar{b}$ ($t\bar{t}$) final state increases (decreases) with increasing $\tan\beta$. This qualitative behavior is seen in Fig. 6 where the size of the Higgs-dominated region decreases with increasing $\tan\beta$. The effect of the top quark shows up dramatically in Fig. 6 where fermion channels dominate along the top quark mass threshold when the top is heavy. When M is small, corresponding to a "B-ino–like" state, the relevant couplings for $\tilde{\chi}\tilde{\chi} \to W^+W^-, ZZ$ are small (see Appendixes A and B) and the gauge-boson final states are unimportant.

For a neutralino that is either gaugino- or Higgsino-like, the Higgs couplings are mostly small and those that are non-negligible appear in diagrams where heavy virtual particles (heavier neutralinos) are exchanged, so annihilation into Higgs final states is relatively small. For a neutralino state that is neither pure gaugino nor pure Higgsino ("mixed state"), Higgs channels become more important but our numerical results suggest that these final states never dominate for very heavy ($m_{\tilde{\chi}} \gg m_W$) neutralinos. In the "mixed state" regions, several final states generally contribute comparable amounts to the total cross section. We remind the reader once again that in Fig. 6 the importance of the new channels

has been *underestimated* since we have set $m_{\tilde{f}} = m_{\tilde{\chi}}$; of course, in general $m_{\tilde{f}}$ should be greater than $m_{\tilde{\chi}}$—and $m_{\tilde{f}}$ could be much greater than $m_{\tilde{\chi}}$.

To illustrate the squark-mass dependence of our results, we set $m_{\tilde{f}} = 2m_{\tilde{\chi}}$ in Fig. 7. As expected, the regions of domination by fermion final states shrink and the regions of Higgs domination and those where no single channel dominates grow. In Fig. 8, we minimize the effect of the fermion channels by setting $m_{\tilde{f}} = \infty$, the opposite extreme of $m_{\tilde{f}} = m_{\tilde{\chi}}$. Even though fermions can still be produced via a Z or Higgs-boson exchange, we see that fermion final states hardly ever dominate in this limit. It is also seen that the Higgs final states are more important for B-ino annihilation, while gauge-boson channels dominate for Higgsino states.

As just mentioned, these cross sections can also be used for neutralino annihilation in the galactic halo or in the body of the Sun or Earth. There are several interesting possibilities for detecting the products from such annihilations.[2] In these cases, the limit $v \to 0$ is appropriate and the formulas simplify considerably. The cross sections in this limit are displayed in the Appendixes, Eqs. (A10), (B7), (C11), and (D6).

III. COSMOLOGICAL CONSTRAINTS

Using the cross sections discussed in Section II and given in the Appendixes, the relic abundance of neutralinos can be found by integrating the Boltzmann equation,

$$\frac{dn_{\tilde{\chi}}}{dt} + 3Hn_{\tilde{\chi}} = -\langle \sigma v \rangle \left[n_{\tilde{\chi}}^2 - (n_{\tilde{\chi}}^{eq})^2 \right], \tag{2}$$

where $n_{\tilde{\chi}}$ is the actual number density of neutralinos, $n_{\tilde{\chi}}^{eq}$ is the equilibrium number density, H is the expansion rate of the Universe, and $\langle \sigma v \rangle$ is the total annihilation cross section, thermally averaged and averaged over initial neutralino spins. Qualitatively, the number density of neutralinos tracks its equilibrium value until the annihilation rate $\Gamma = n_{\tilde{\chi}} \langle \sigma v \rangle$, drops below the expansion rate H ("freeze-out"), after which a relic abundance of neutralinos "freezes-in." The freeze-out temperature T_f depends logarithmically upon $\langle \sigma v \rangle$, but generally occurs for a value $x_f = m_{\tilde{\chi}}/T_f \approx \mathcal{O}(20\text{-}30)$.

While it is straightforward to integrate Eq. (2) numerically, because of the large number of times we must do so, it is far more convenient to use an analytic approximation (good to about 5-10%) for the relic abundance instead. In this regard we have generally followed the treatment detailed in Ref. 15.

After freeze-in, the neutralino abundance per comoving volume no longer drops rapidly and it is therefore convenient to rewrite the Boltzmann equation using the variable $Y = n_{\tilde{\chi}}/s$, where $s = 2\pi^2 g_* T^3/45$ is the entropy density and g_* counts the total number of effectively relativistic degrees of freedom. Then the fraction of critical density contributed by relic neutralinos today is given by

$$\begin{aligned} \Omega_{\tilde{\chi}} h^2 &= \frac{\rho_{\tilde{\chi}}}{\rho_{\rm crit}/h^2} = \frac{Y_\infty s_0 m_{\tilde{\chi}}}{\rho_{\rm crit}/h^2} \\ &\approx 2.82 \times 10^8 \; Y_\infty (m_{\tilde{\chi}}/{\rm GeV}), \end{aligned} \tag{3}$$

where the present critical density is $\rho_{\rm crit} = 1.05 \times 10^4 \; h^2$ eV cm^{-3}, the present Hubble constant is 100 h km sec^{-1} Mpc^{-1} with $0.4 \leq h \leq 1$, and the present entropy density is $s_0 = 2970$ cm^{-3}.

Expanding the total annihilation cross section in powers of the neutralino relative velocity,

$$\sigma v = a + b v^2 + \cdots, \tag{4}$$

it can be shown that an accurate approximation to the neutralino relic abundance is given by

$$Y_\infty^{-1} = 0.264 g_*^{1/2} m_{Pl} m_{\tilde{\chi}} \left\{ \frac{a}{x_f} + \frac{3b}{x_f^2} \right\}. \tag{5}$$

The freeze-out epoch x_f is determined by

$$x_f = \ln \frac{0.0764 \; m_{Pl}(a + 6b/x_f) c(2+c) m_{\tilde{\chi}}}{\sqrt{g_*} x_f^{1/2}}, \tag{6}$$

which can be solved iteratively to the required precision. Here $m_{Pl} = 1.22 \times 10^{19}$ GeV is the Planck mass and c is a constant of order unity whose value is determined by matching the approximate analytic solutions for $x \lesssim x_f$ and

$x \gtrsim x_f$. In practice, once chooses c to obtain the most accurate approximation to Y_∞; we have used the value $c = 1/2$ which results in a typical accuracy of about 5-10%—more than sufficient for our purposes here.

Figs. 9, 10, and 11 illustrate the dependence of $\Omega_{\tilde{\chi}} h^2$ on M and μ for $\tan\beta = 2$ and $m_t = 60$ GeV, for several slices through the M-μ plane. The behavior of $\Omega_{\tilde{\chi}} h^2$ depends on the mass and gaugino fraction of the neutralino and the relative importance of the cross sections into the various final states; therefore in the following, the reader is encouraged to frequently refer to Figs. 1, 6, and 8. In Fig. 9, $\Omega_{\tilde{\chi}} h^2$ is shown as a function of M for several values of μ under the two extreme assumptions, $m_{\tilde{f}} = m_{\tilde{\chi}}$ (solid lines) and $m_{\tilde{f}} = \infty$ (broken lines). Assuming $m_{\tilde{f}} = m_{\tilde{\chi}}$, the relic abundance grows with increasing M (and therefore increasing $m_{\tilde{\chi}}$ (Fig. 1)) while the neutralino is mostly B-ino (Fig. 6) and the fermion channels dominate (Fig. 6). This is because $\Omega_{\tilde{\chi}} \sim \langle\sigma v\rangle^{-1} \sim m_{\tilde{f}}^4/{m_{\tilde{\chi}}}^2 \sim {m_{\tilde{\chi}}}^2$, due to our assumption that $m_{\tilde{f}} = m_{\tilde{\chi}}$. The neutralino mass density $\Omega_{\tilde{\chi}} h^2$ reaches a maximum near the value of M where the neutralino is an equal mixture of gaugino and Higgsino and drops quickly as the gauge boson channels begin to dominate and increase the cross section (Fig. 6). For larger M, the neutralino is mostly Higgsino and its mass does not change as M increases further (Fig. 1), so $\Omega_{\tilde{\chi}} h^2$ levels off.

The broken curve in Fig. 9 is similar to the solid curve except that we have set $m_{\tilde{f}} = \infty$, greatly suppressing the fermion channels (Fig. 8). For small M, the neutralino is B-ino–like (Fig. 1) and annihilates primarily into Higgs bosons (Fig. 8). Since $\Omega_{\tilde{\chi}} h^2$ stays nearly constant, we can conclude that the cross section in this region is nearly independent of $m_{\tilde{\chi}}$. In fact, examination of the cross section given in Appendix C shows that annihilation is completely dominated by the exchange of the *heaviest* neutralino which is very nearly a pure Higgsino. (Exchange of the lighter neutralinos is suppressed due to the lack of a B-ino–B-ino–Higgs coupling.) Since the mass of the heaviest neutralino is very nearly equal to μ, we find a cross section that is proportional to μ^{-2}. For large M, the behavior is determined again by annihilation into gauge bosons and the suppression of the fermion channels due to large $m_{\tilde{f}}$ makes no difference.

In Fig. 10, we show $\Omega_{\tilde{\chi}}h^2$ for three slices through the M-μ plane with M held constant as μ increases, again for $m_{\tilde{f}} = m_{\tilde{\chi}}$ (solid lines) and $m_{\tilde{f}} = \infty$ (broken lines). For small μ, the neutralino is mostly Higgsino (Fig. 1), annihilates primarily into gauge bosons (Fig. 6), and $m_{\tilde{\chi}}$ increases with μ (Fig. 1). Again $\Omega_{\tilde{\chi}}h^2 \sim (\sigma v)^{-1} \sim s^2/m_{\tilde{\chi}}{}^2 \sim m_{\tilde{\chi}}{}^2$. Now, however, the switch to a higgsino annihilating into fermions results in a jump in $\Omega_{\tilde{\chi}}h^2$ (rather than a drop as in Fig. 9). Again, for $m_{\tilde{f}} = m_{\tilde{\chi}}$ (the solid curves) and large values of μ, $\Omega_{\tilde{\chi}}h^2$ levels off because $m_{\tilde{\chi}}$ becomes constant for large μ. The broken curves in Fig. 10 show $\Omega_{\tilde{\chi}}h^2$ when $m_{\tilde{f}} = \infty$, and we find that at small μ, the behavior is similar to the case where $m_{\tilde{f}} = m_{\tilde{\chi}}$. As μ increases further, the neutralino becomes B-ino–like, and annihilation into Higgs bosons dominates (the fermion channels being suppressed by $m_{\tilde{f}} = \infty$). The relic abundance increases with μ because $\langle\sigma v\rangle \sim \mu^{-2}$ as mentioned earlier.

Finally, in Fig. 11 we show a slice of the M-μ plane along the line $\mu = \frac{5}{3}M\tan^2\theta_W$ (which for large μ corresponds to a neutralino that is an equal Higgsino-gaugino mixture) for $m_{\tilde{f}} = m_{\tilde{\chi}}$ (solid line) and $m_{\tilde{f}} = \infty$ (broken line). For small μ, the relic abundance dips as new annihilation channels become kinematically allowed; however, as seen in Fig. 1, $m_{\tilde{\chi}}$ increases monotonically along this line when the neutralino becomes heavy, and $\Omega_{\tilde{\chi}}h^2$ increases with increasing $m_{\tilde{\chi}}$, as it should. As expected from Fig. 6, the relic abundance for $m_{\tilde{f}} = \infty$ is slightly higher than that for $m_{\tilde{f}} = m_{\tilde{\chi}}$ since the fermion and gauge-boson contributions are generally of the same order of magnitude for a neutralino that is an equal Higgsino-gaugino mixture.

The results shown in Figs. 9-11 are qualitatively the same for $\mu < 0$ and other values of $\tan\beta$ and m_t.

The age of the Universe at the present epoch (specified by a photon temperature $T = 2.75$ K) decreases with increasing values of Ωh^2. If one insists that the age of the Universe today is greater than 10 Gyr and that $h \gtrsim 0.4$, the cosmological bound $\Omega_{\tilde{\chi}}h^2 < \Omega h^2 \lesssim 1$ follows.[15] We now use this limit, $\Omega_{\tilde{\chi}}h^2 \lesssim 1$, to exclude regions of the M, μ, $\tan\beta$ parameter space. As mentioned earlier, raising $m_{\tilde{f}}$ lowers the annihilation rate which in turn increases the relic abundance.

Therefore we set $m_{\tilde{f}} = m_{\tilde{\chi}}$, so that regions of parameter space are excluded independently of the unknown squark mass.

In order to provide realistic limits, we will consider top quark masses in the range 60 GeV $\leq m_t \leq$ 180 GeV. The lower bound follows from unsuccessful experimental searches,[16] and the upper bound follows from limits on radiative corrrections to $\sin^2\theta_W$ (Ref. 17). The range of $\tan\beta$ considered is $1 < \tan\beta < m_t/m_b$. The reason is that for $m_t \gg m_b$, radiative corrections drive $\tan\beta = v_2/v_1$ to a value greater than 1. In addition, in many supergravity models, electroweak symmetry breaking only occurs if $\tan\beta < m_t/m_b$ (Ref. 18).

In Fig. 12, we have hatched out the regions of the M-μ plane (for $\tan\beta = 2$) that are cosmologically excluded for our limiting cases, $m_t = 60$ GeV and 180 GeV. (The results for other values of $\tan\beta$ are qualitatively similar. The excluded regions for $\mu < 0$ are similar to those for $\mu > 0$ and so are not shown.) From Fig. 12 we see that a Higgsino-like neutralino is constrained to be less massive than about 3000 GeV; on the other hand, a B-ino–like neutralino must be less massive than about 550 GeV. Note that both bounds become more stringent as m_t decreases.

To illustrate the dependence of our results on the assumption that $m_{\tilde{f}} = m_{\tilde{\chi}}$, we show in Fig. 13 the cosmologically excluded regions for $m_{\tilde{f}} = \infty$. The region of Higgsino-like parameter space excluded is very similar to the case shown in Fig. 12, but many more B-ino–like states are excluded. This is because the fermion annihilation channels are (are not) important for a B-ino- (Higgsino-) like neutralino.

As the neutralino mass becomes large, the annihilation cross section decreases. Therefore, the constraint $\Omega_{\tilde{\chi}}h^2 \lesssim 1$ leads to a maximum cosmologically acceptable neutralino mass. In order to find the maximum neutralino mass consistent with cosmology we must search the parameter space of M, μ, $\tan\beta$, and m_t. We did so as follows. For a given m_t and $\tan\beta$, the M-μ plane was searched numerically for the largest value of $m_{\tilde{\chi}}$ consistent with $\Omega_{\tilde{\chi}}h^2 \lesssim 1$. For $m_t = 60$ GeV, the heaviest possible neutralino is mostly Higgsino, and neutralino annihilation proceeds mainly into gauge bosons. For larger values of m_t,

the heaviest possible neutralino is nearly half Higgsino and half gaugino, and the fermion annihilation channels are of comparable importance. In Fig. 14, the maximum cosmologically acceptable neutralino mass is shown as a function of $\tan\beta$ for several values of m_t. As mentioned before, we consider values of $\tan\beta$ between 1 and m_t/m_b. From Fig. 14 we see that for $m_t < 180$ GeV,[17] a neutralino mass greater than 3200 GeV is cosmologically unacceptable. If the top quark mass should be about 120 GeV, then the neutralino must have a mass less than around 2600 GeV. It is interesting that the cosmological window for the neutralino mass roughly coincides with that for solving the hierarchy problem.[8] These neutralino mass limits would weaken if larger values of m_t or more extreme values of $\tan\beta$ were allowed; we believe, however, that we have been generous in the regions of parameter space explored.

Finally, we should mention the status of the "pure" photino and "pure" Higgsino states which are frequently considered in the literature as dark matter candidates. A pure photino is defined as $Z_{n1} = \cos\theta_W$, $Z_{n2} = \sin\theta_W$, and $Z_{n3} = Z_{n4} = 0$, while the Higgsino usually considered has $Z_{n1} = Z_{n2} = 0$, $Z_{n3} = \sin\beta$, and $Z_{n4} = \cos\beta$. When the neutralino is light, an LSP state that is a pure photino plus a correction of order $m_{\tilde{\gamma}}{}^2/m_W^2$ (where $m_{\tilde{\gamma}}$ is the photino mass) exists, and is in fact common. Likewise, in the low mass limit there is a state that is close to the Higgsino state defined above. Usually however, the above relations are assumed to hold without regard to the neutralino mass matrix from which they arise. In fact, given the unification assumption, $M' = \frac{5}{3}M\tan^2\theta_W$, an examination of the mass matrix shows that neither of these states exists as the LSP for $m_{\tilde{\chi}} > m_W$. If the unification assumption is relaxed, a photino-like state of any mass is possible and the relic abundance for these massive photinos can be calculated in the same manner as for massive neutralinos. Using $m_{\tilde{f}} < m_{\tilde{\gamma}}$, $m_t < 180$ GeV, and $\Omega h^2 < 1$, one finds a maximum photino mass of around 600 GeV, a number very similar to our limit for the more realistic B-ino state. For the Higgsino state defined above, the crucial Z-Higgsino-Higgsino coupling becomes $Z_{n3}^2 - Z_{n4}^2 = \cos^2 2\beta$ and such a state annihilates with the cross section of a Majorana neutrino times the factor $\cos^2 2\beta$. For large mass however, this particular Higgsino solution no longer occurs, and as discussed previously, the

actual large mass Higgsino-like solution has $Z_{n3} \approx \pm Z_{n4}$. So we conclude that for discussion of supersymmetric dark matter above the W mass, the photino and Higgsino states that are usually considered are not so relevant.

In closing this section, we should again remind the reader that implicit in our calculation of $\Omega_{\tilde{\chi}} h^2$ was the assumption that there was no significant entropy production *after* the freeze-out of the relic abundances. If there were significant entropy production—*e.g.*, due to the quark/hadron transition, electroweak symmetry breaking, or relic particle decays—and the entropy per comoving volume increased by a factor of γ, then our estimate for $\Omega_{\tilde{\chi}} h^2$ would decrease by the same factor of γ. On the other hand, our cosmological upper bound to $\Omega_{\tilde{\chi}} h^2$ is rather generous: Had we assumed that the Universe today must be at least 13 Gyr old—a very reasonable lower bound—the cosmological upper limit to $\Omega_{\tilde{\chi}} h^2$ would fall to about 0.4. Or if we insist that $\Omega = 1$ and that the age of the Universe be at least 10 Gyr, then $h \lesssim 0.7$, and $\Omega_{\tilde{\chi}} h^2 \lesssim 0.5$.

IV. HEAVY NEUTRALINOS AS DARK MATTER CANDIDATES

It should be noted that for almost any value of M and μ not cosmologically excluded, a relic neutralino abundance of significance for the dark matter problem, say $0.025 \lesssim \Omega_{\tilde{\chi}} h^2 \lesssim 1$, can result. These models are interesting because they offer an elegant solution to the dark matter problem and predict the existence of particles in our galactic halo which may be detectable.[19]

In Fig. 15, we show "scatter" plots of $\Omega_{\tilde{\chi}} h^2$ vs. $m_{\tilde{\chi}}$ for models taken from a grid of points in the M-μ plane. For light neutralinos ($m_{\tilde{\chi}} < m_W$), the relic abundances displayed *underestimate* the expected values because we set $m_{\tilde{f}} = m_{\tilde{\chi}}$. Since the cross section for annihilation into fermions $(\sigma v)_{f\bar{f}} \sim (m_{\tilde{f}}^2 + m_{\tilde{\chi}}^2)^{-2}$, if the squark is x times heavier than the neutralino, the relic abundance for light neutralinos is about a factor of $(x^2+1)^2/4$ larger than that shown in Fig. 15 (assuming the Higgs channels are negligible).[5] Some indication of this fact can be seen in Fig. 16 where we have set $m_{\tilde{f}} = 2m_{\tilde{\chi}}$. As expected, the relic abundance for neutralinos that are mostly B-ino increases roughly as described above. For reference, the relic abundances that result when we set $m_{\tilde{f}} = \infty$ are shown in Fig. 17. In Figs. 15, 16, and 17 we arbitrarily set $m_{H_2^0} = 0$ since for heavy neu-

tralinos, the relic abundance is insensitive to this parameter. For light neutralinos this is not the case.[9]

Now consider the relic abundance of very heavy neutralinos. Note that for large masses, the relic neutralino abundance seems to cluster along two lines. Along the upper line, the neutralino is mostly B-ino. Since annihilation for a B-ino–like neutralino is dominated by the fermion channels, one would generally expect a relic abundance higher than shown here (where $m_{\tilde{f}} = m_{\tilde{\chi}}$). This is seen in Figs. 16 and 17 where an increase in $m_{\tilde{f}}$ results in larger values of $\Omega_{\tilde{\chi}} h^2$. For a B-ino–like neutralino, $\Omega_{\tilde{\chi}} \sim 1$ occurs for a neutralino mass of around 100-300 GeV.

Along the lower line in Fig. 15 the neutralino is mostly Higgsino. In this region, the gauge-boson annihilation channels dominate the total annihilation cross section and the results do not depend upon the assumed value of $m_{\tilde{f}}/m_{\tilde{\chi}}$; *cf.* Figs. 15-17. However, if the top quark is very heavy ($m_t \approx 180$ GeV) the fermion annihilation channels become comparable to the gauge-boson channels, even for a Higgsino-like neutralino. In this case the importance of the fermion annihilation channels will depend upon $m_{\tilde{f}}/m_{\tilde{\chi}}$: if this ratio is sufficiently large, the gauge-boson channels will still dominate. The fact that the Higgsino curves in Figs. 15(a), 16, and 17 are the same illustrates this point. In any case, the "Higgsino line" in Fig. 17 provides an upper bound to $\Omega_{\tilde{\chi}} h^2$ for Higgsino-like neutralinos, independent of m_t and $m_{\tilde{f}}$. Note also that our results indicate that a Higgsino-like heavy neutralino also provides a viable dark matter candidate for a wide range of neutralino masses.

If $\Omega_{\tilde{\chi}} h^2 \lesssim 0.025$, it is unlikely that the neutralino is the primary component of the dark matter. However, such neutralinos would still reside in our galactic halo as a minor component of the dark matter and might still be detectable. We should remind the reader that there are few cosmological relics, and even relics that contribute only a small fraction of critical density are very interesting. Moreover, independent of whether or not the relic neutralinos are the primary component of the dark matter, if detected, they still could provide the first evidence for supersymmetry!

Unfortunately, a heavier neutralino is more difficult to detect because for fixed mass density, the number density is lower for heavier particles. In addition, the matrix element for the interaction of a neutralino—or any dark matter particle—is typically related to the annihilation matrix element by crossing symmetry, and the annihilation cross section for particle dark matter is always of order 10^{-27} cm^3 sec^{-1}.[20] Since, roughly speaking, the rate for direct detection is proportional to the interaction cross section with matter times the relic number density and the number density is proportional to $(m_{\tilde{\chi}})^{-1}$, the rate for direct detection is generally inversely proportional to $m_{\tilde{\chi}}$.[19,20] Likewise, indirect detection schemes—searching for the annihilation products of neutralinos that annihilate in the halo, in the Sun, or in the Earth—depend upon the annihilation cross section times the square of the number density. This implies that for fixed $\Omega_{\tilde{\chi}}$, the rate for annihilation in the galactic halo falls off roughly as $m_{\tilde{\chi}}{}^{-2}$. On the other hand, the energy of the decay products increases with increasing $m_{\tilde{\chi}}$ and the backgrounds at higher energies tend to be smaller.

To be more quantitative about indirect detection, in Fig. 18 we show a scatter plot of the volume annihilation rate $\Gamma_{\rm halo}$ for neutralinos in the galactic halo as a function of the neutralino mass for a wide range of supersymmetric models. To simplify matters, we have assumed that $m_t = 60$ GeV, $\tan\beta = 2$, and $m_{H_2^0} = 0$, and have used both $m_{\tilde{f}} = m_{\tilde{\chi}}$ and $m_{\tilde{f}} = \infty$. Further, we have selected values of μ and M from a grid in the M-μ plane and eliminated models where $\Omega_{\tilde{\chi}} h^2 \gtrsim 1$. For the local number density of neutralinos $n_{\tilde{\chi}}$, we have used the following simple model. For $\Omega_{\tilde{\chi}} \gtrsim \Omega_{\rm halo}$, it is reasonable to assume that neutralinos comprise the halo dark matter and thus $n_{\tilde{\chi}} = \rho_{\rm halo}/m_{\tilde{\chi}}$. For $\Omega_{\tilde{\chi}} \lesssim \Omega_{\rm halo}$, it is very unlikely that neutralinos comprise the bulk of the halo dark matter; as a simple model we suppose that $n_{\tilde{\chi}} = (\Omega_{\tilde{\chi}}/\Omega_{\rm halo})(\rho_{\rm halo}/m_{\tilde{\chi}})$. The second case corresponds to the situation where neutralinos are a "minor"—but potentially interesting—component of the halo. To smoothly interpolate between these two cases, we have used the simple ansatz,

$$n_{\tilde{\chi}} = \frac{\rho_{\rm halo}/m_{\tilde{\chi}}}{1 + \Omega_{\rm halo} h^2/\Omega_{\tilde{\chi}} h^2}. \tag{7}$$

For $\rho_{\rm halo}$ we use 0.3 GeV cm^{-3}. Based upon the rotation curves of spiral galaxies $\Omega_{\rm halo} \simeq$ 0.03-0.1 (or greater since there is no convincing evidence for the convergence of the halo mass of any spiral galaxy); for definiteness we have taken $\Omega_{\rm halo}h^2 = 0.03$. The volume rate for neutralino annihilations in the galactic halo is then $\Gamma_{\rm halo} = n_{\tilde{\chi}}^2 \langle \sigma v \rangle|_{v=0}$. One can see that the galactic annihilation rate varies roughly as $m_{\tilde{\chi}}{}^{-2}$ (as argued above). By using $m_{H_2^0} = 0$, we eliminate the well-known s-wave suppression for light neutralino annihilation at zero velocity;[13] therefore, the galactic annihilation rates for light neutralinos for larger values of $m_{H_2^0}$ will generally be smaller than those shown in Fig. 18. An interesting consequence of our model for galactic neutralino abundance is that the galactic annihilation rate does not necessarily decrease with decreasing relic abundance; this is because $\Omega_{\tilde{\chi}}h^2 \propto \langle \sigma v \rangle^{-1}$ and for $\Omega_{\tilde{\chi}} \gtrsim \Omega_{\rm halo}$, we have fixed $n_{\tilde{\chi}}$. Thus, even a neutralino that fails to solve the dark matter problem may prove to be an interesting candidate for indirect detection. Of course, here we have only considered the rate for neutralino annihilation in the galactic halo. To find expected experimental signatures, the branching ratios for specific final states (*e.g.*, positrons, neutrinos, etc.) and the propagation of these annihilation products must also be considered.[9]

V. CONCLUSIONS

In this paper, we have studied in some detail the possibility of a "heavy" neutralino ($m_{\tilde{\chi}} > m_W$), mapping out completely the cosmologically allowed regions of parameter space. The main difference between a heavy and a light ($m_{\tilde{\chi}} < m_W$) neutralino is that additional annihilation channels open up (various pairs of Higgs and gauge bosons) which have not been included in the previous treatments[4,5] (apart from a recent report of Srednicki and Olive[6]). We have calculated the annihilation cross sections into these new channels for a general neutralino state. In large regions of the parameter space for the minimal supersymmetric extension of the standard model (μ, M, $\tan\beta$, $m_{H_2^0}$, $m_{\tilde{f}}$, and m_t) the new channels make a substantial contribution to the annihilation cross section, and for a neutralino that is Higgsino-like, the gauge-boson final states (W^+W^-, ZZ) often dominate all the other channels by a factor of ten. On the other hand, for a heavy neu-

tralino that is gaugino-like, the new final states are typically sub-dominant. The new channels contribute and cannot be ignored for neutralinos that are mixed states.

Using our results for the new annihilation channels along with previous results for the fermion final states, we have calculated the total annihilation cross section for heavy neutralinos and from this, the relic cosmological abundance of heavy neutralinos. We find that for a large portion of the parameter space, a heavy neutralino of mass between m_W and 3200 GeV can have a cosmologically interesting relic abundance, *i.e.*, $0.025 \lesssim \Omega_{\tilde{\chi}} h^2 \lesssim 1$. Thus, we conclude that a heavy neutralino is a well motivated and viable dark matter candidate. Based upon the cosmological constraint $\Omega_{\tilde{\chi}} h^2 \lesssim 1$, we have mapped out the regions of parameter space that are cosmologically forbidden. In particular, for $m_t < 180$ GeV, one can completely rule out a neutralino that is heavier than about 3200 GeV. For a neutralino that is Higgsino-like, the bound is about 3000 GeV, while if the neutralino is gaugino-like, the bound is about 550 GeV. (If a top quark of mass less than 120 GeV is discovered, the general bound drops to 2600 GeV.) It is interesting to note that the cosmological upper bound to the neutralino mass is comparable to that which follows by insisting that low-energy supersymmetry "solve" the hierarchy problem.

ACKNOWLEDGEMENTS

MPK would like to thank R. G. Sachs for encouragement during the early part of this work. This research was supported in part by the DoE (at Chicago), by NASA (grant NGW-1340) and the DoE at Fermilab, and by the NSF Office of Science and Technology Centers, under cooperative agreement AST-8809616 (at Berkeley). MPK also acknowledges financial support through the NASA Graduate Student Research Program.

APPENDIX A: CROSS SECTION FOR $\widetilde{\chi}\widetilde{\chi} \to W^+W^-$

First let us review the masses and mixing parameters of the minimal supersymmetric standard model. The quantities M, M', and μ are the masses that appear in the neutralino mass matrix, Y, Eq. (C38) of Ref. 1, and Z_{ij} are the

elements of the *real* orthogonal matrix that diagonalizes Y. The masses of the four neutralinos are the absolute values of the eigenvalues of Y, $m_{\tilde{\chi}_i^0}$; one should keep in mind the fact that the $m_{\tilde{\chi}_i^0}$ *may* be negative. The mass of the lightest neutralino is the n^{th} eigenvalue of Y which we shall denote by $m_{\tilde{\chi}}$. The chargino masses $m_{\tilde{\chi}_i^+}$, given by Eq. (C18) in Ref. 1, are ***always positive***. The quantities ϕ_- and ϕ_+, determined from formulas given in Ref. 21, describe the mixing of the charginos. The squares of the Higgs-boson masses ($m^2_{H_1^0}$ and $m^2_{H_2^0}$), α, and β are given in Appendix A of Ref. 12. Finally, the quantities g and g' are respectively the $U(1)$ and $SU(2)$ gauge couplings. In this Appendix only, some quantities are scaled by m_W in order to simplify some of the equations. Specifically,

$$\omega = \left(\frac{m_{\tilde{\chi}}}{m_W}\right)^2; \quad \kappa_i = \left(\frac{m_{\tilde{\chi}_i^+}}{m_W}\right)^2; \quad \zeta = \left(\frac{m_Z}{m_W}\right)^2; \quad s = \frac{(p_1+p_2)^2}{m_W^2}, \tag{A1}$$

where sm_W^2 is the square of the center of mass energy, and p_1 and p_2 are the four-momenta of the incoming neutralinos. (In Appendix B, these same quantities will be rescaled by m_Z.)

Next we define the quantities

$$\begin{aligned}
\begin{pmatrix} e_1 \\ e_2 \end{pmatrix} &= 2\left[\frac{Z_{n3}}{\sqrt{2}}\begin{pmatrix} \sin\phi_- \\ \cos\phi_- \end{pmatrix} + Z_{n2}\begin{pmatrix} \cos\phi_- \\ -\sin\phi_- \end{pmatrix}\right], \\
\begin{pmatrix} f1 \\ f_2 \end{pmatrix} &= 2\left[\frac{-Z_{n4}}{\sqrt{2}}\begin{pmatrix} \sin\phi_+ \\ \epsilon\cos\phi+ \end{pmatrix} + Z_{n2}\begin{pmatrix} \cos\phi_+ \\ -\epsilon\sin\phi_+ \end{pmatrix}\right],
\end{aligned} \tag{A2}$$

where $\epsilon = \frac{\det X}{|\det X|}$ and X is the matrix defined in Eq. (C9) of Ref. 1. From these we define

$$\begin{aligned}
C_i^{(1)} &= e_i^2 f_i^2, \qquad C_i^{(2)} = e_i^3 f_i + e_i f_i^3, \\
C_i^{(3)} &= e_i^4 + f_i^4, \qquad C_i^{(5)} = e_i^2 - f_i^2, \qquad C_i^{(6)} = e_i^2 + f_i^2, \\
D^{(1)} &= e_1^2 e_2^2 + f_1^2 f_2^2, \qquad D^{(2)} = e_2^2 e_1 f_1 + f_2^2 e_1 f_1, \\
D^{(3)} &= e_1^2 f_2^2 + e_2^2 f_1^2, \qquad D^{(4)} = e_1^2 e_2 f_2 + f_1^2 e_2 f_2, \\
D^{(5)} &= 2 e_1 e_2 f_1 f_2,
\end{aligned} \tag{A3}$$

where $i = 1, 2$.

The following dimensionless quantities are also useful,

$$\begin{aligned}
\gamma &= \sqrt{(1-\frac{4\omega}{s})(1-\frac{4}{s})}, \\
L_i &= \frac{1}{\gamma s}\log\left[\frac{(1+\gamma)s-2-2\omega+2\kappa_i}{(1-\gamma)s-2-2\omega+2\kappa_i}\right], \\
K_i &= \frac{1}{\gamma s}\left[\frac{1}{(1+\gamma)s-2-2\omega+2\kappa_i}-\frac{1}{(1-\gamma)s-2-2\omega+2\kappa_i}\right], \\
A &= \frac{m_{\tilde{\chi}}}{m_W}\sin\alpha+2\left[Q\sin(\beta-\alpha)-R\sin\alpha\right], \\
C &= \frac{m_{\tilde{\chi}}}{m_W}\cos\alpha-2\left[Q\cos(\beta-\alpha)+R\cos\alpha\right],
\end{aligned} \tag{A4}$$

where

$$\begin{aligned}
Q = \frac{Z_{n3}}{g}(gZ_{n2}-g'Z_{n1}), \qquad R &= \frac{1}{2m_W}(MZ_{n2}^2+M'Z_{n1}^2-2\mu Z_{n3}Z_{n4}), \\
F &= Z_{n3}^2-Z_{n4}^2.
\end{aligned} \tag{A5}$$

The total cross section, averaged over neutralino spin for the process $\widetilde{\chi}\widetilde{\chi} \to W^+W^-$ is given by

$$\begin{aligned}
\sigma_{WW} =& \frac{1}{32\pi s m_W^2}\left(\frac{s-4}{s-4\omega}\right)^{\frac{1}{2}} \\
&\times\left(X_{ZZ}+X_{HH}+X_{\widetilde{\chi}^+\widetilde{\chi}^+}+X_{\widetilde{\chi}^+{}_i\widetilde{\chi}^+}+X_{Z\widetilde{\chi}^+}+X_{H\widetilde{\chi}^+}\right).
\end{aligned} \tag{A6}$$

The quantities X_{ii} arise from squaring the matrix element given by the Feynman diagrams in Fig. 2, summing over final state polarizations and averaging over initial neutralino spins. Specifically, X_{ZZ} comes from the square of the Z-exchange diagram, X_{HH} comes from the square of the Higgs exchange diagrams, $X_{\widetilde{\chi}^+\widetilde{\chi}^+}$ comes from the sum of the squares of the t- and u-channel exchange of the charginos, $X_{\widetilde{\chi}^+{}_i\widetilde{\chi}^+}$ comes from the interference between the t- and u-channel exchange of the charginos, and $X_{Z\widetilde{\chi}^+}$ and $X_{H\widetilde{\chi}^+}$ come from the interference of the chargino exchange diagrams with the Z and Higgs exchange diagrams. The interference between the Z and Higgs exchange diagram vanishes. The quantities

X_{ii} are given by

$$
\begin{aligned}
X_{ZZ} &= \frac{g^4F^2}{24}\frac{(s-4)(s-4\omega)(s^2+20s+12)}{(s-\zeta)^2+(\Gamma_Z/m_Z)^2}, \\
X_{HH} &= \frac{g^4}{8\sin^2\beta}\left[2+(\frac{s}{2}-1)^2\right](s-4\omega)A'^2, \\
X_{\widetilde{\chi}^+\widetilde{\chi}^+} &= \frac{g^4}{16}\sum_i\left(C_i^{(1)}G_i^{(1)}+\frac{m_{\tilde{\chi}_i^+}}{m_W}\frac{m_{\tilde{\chi}}}{m_W}C_i^{(2)}G_i^{(2)}+C_i^{(3)}G_i^{(3)}\right), \\
X_{\widetilde{\chi}^+i\widetilde{\chi}^+} &= \frac{g^4}{8}\Bigg[D^{(1)}G^{(4)}+\frac{m_{\tilde{\chi}}}{m_W}\left(\frac{m_{\tilde{\chi}_1^+}}{m_W}D^{(2)}+\frac{m_{\tilde{\chi}_2^+}}{m_W}D^{(4)}\right)G^{(5)}-D^{(3)}G^{(6)} \\
&\qquad\qquad +\frac{m_{\tilde{\chi}_1^+}}{m_W}\frac{m_{\tilde{\chi}_2^+}}{m_W}D^{(5)}G^{(7)}\Bigg], \\
X_{Z\widetilde{\chi}^+} &= \frac{g^4F}{8\left[(s-\zeta)^2+(\Gamma_Z/m_Z)^2\right]^{1/2}}\sum_i C_i^{(5)}G_i^{(8)}, \\
X_{H\widetilde{\chi}^+} &= \frac{-g^4A'}{8\sin\beta}\sum_i\left(\frac{m_{\tilde{\chi}}}{m_W}C_i^{(6)}G_i^{(9)}+2\frac{m_{\tilde{\chi}_i^+}}{m_W}e_if_iG_i^{(10)}\right),
\end{aligned}
\tag{A7}
$$

where Γ_Z is the Z width. Here

$$
A' = \frac{A\cos(\beta-\alpha)}{\left[(s-m_{H_1^0}^2/m_W^2)^2+(\Gamma_{H_1^0}/m_W)^2\right]^{1/2}}+\frac{C\sin(\beta-\alpha)}{\left[(s-m_{H_2^0}^2/m_W^2)^2+(\Gamma_{H_2^0}/m_W)^2\right]^{1/2}},
\tag{A8}
$$

where $\Gamma_{H_i^0}$ is the width of the H_i^0, and the G are given by

$$
\begin{aligned}
G_i^{(1)} =& 4\kappa_iK_i\left[-(\kappa_i-\omega-2)^2s+4(\kappa_i-\omega-1)^2+2\omega+36\right] \\
&-\frac{1}{6}\left[2s^2+s(40-8\omega-36\kappa_i)+24\omega-12(\kappa_i-\omega)^2+120\kappa_i\right] \\
&+4L_i\left[s^2(4\kappa_i-2\kappa_i^2-\kappa_i\omega)\right. \\
&+s(8-9\kappa_i-12\omega+14\kappa_i^2-6\omega\kappa_i+4\omega^2-3\kappa_i(\kappa_i-\omega)^2) \\
&\left.+6\kappa_i-8\omega+9\omega^2-13\kappa_i^2+6\omega\kappa_i+8\kappa_i(\kappa_i-\omega)^2-(\kappa_i-\omega)^4\right], \\
G_i^{(2)} =& 24K_i\left[2-(\kappa_i+\omega)^2-(\kappa_i-\omega)^2\right]+16-4s \\
&+\frac{8L_i}{s-2-2\omega+2\kappa_i}\Big\{s^2(\kappa_i-1)+s\left[(\kappa_i-\omega)^2-6\kappa_i+2\omega+4\right] \\
&-7(\kappa_i-\omega)^2+5\kappa_i-7\omega+2\Big\},
\end{aligned}
$$

$$
\begin{aligned}
G_i^{(3)} =& 2K_i\Big\{\kappa_i\big[(\kappa_i-\omega-2)^2 s+\kappa_i\big[\kappa_i(\kappa_i-4\omega-2)+6\omega^2+6\omega+5\big]\\
&-2(\omega+2)(2\omega^2-\omega+2\big]+(\omega-1)^2(\omega+2)^2\Big\}\\
&+\frac{L_i}{s-2-2\omega+2\kappa_i}\Big\{s^2(3\kappa_i^2+\omega^2-8\kappa_i+4)+2s\big[5\kappa_i^3-(11\omega+14)\kappa_i^2\\
&+(7\omega^2+16\omega+17)\kappa_i-\omega^3-10\omega^2+3\omega-8\big]\\
&+4\big[2(\kappa_i-\omega)^4-4(\kappa_i-\omega)^3-\kappa_i(\kappa_i-\omega)^2\\
&+8\kappa_i^2+9\omega\kappa_i+9\kappa_i-(\omega-4)(\omega+1)\big]\Big\}\\
&-\frac{1}{12}\big[-2s^2+(12\kappa_i-16\omega-40)s+36(\kappa_i-\omega)^2-24\kappa_i+88\omega+48\big],
\end{aligned}
$$

$$
\begin{aligned}
G^{(4)} =& -\frac{L_2}{\kappa_1-\kappa_2}\Big\{s(\kappa_2-\omega-2)^2\kappa_2+(\kappa_2-\omega)^4+2(\omega-\kappa_2)^3\\
&+5\kappa_2^2-8\kappa_2-(\omega+2)(3\omega-2)\Big\}+(1\leftrightarrow 2)\\
&+\frac{\omega L_2}{2+2\omega-\kappa_1-\kappa_2-s}\Big\{\kappa_2 s^2+s\big[(\kappa_2-\omega)^2-6\kappa_2+2\omega-3\big]\\
&-4(\kappa_2-\omega)^2+8\kappa_2+2\omega+2\Big\}+(1\leftrightarrow 2)\\
&-\frac{1}{12}\big[-2s^2+(6\kappa_1+6\kappa_2-16\omega-40)s\\
&+9(\kappa_1+\kappa_2)^2-(36\omega+12)(\kappa_1+\kappa_2)\\
&+3(\kappa_1-\kappa_2)^2+4(9\omega^2+22\omega+12)\big],
\end{aligned}
$$

$$
\begin{aligned}
G^{(5)} =& 8-2s-\frac{6L_2}{\kappa_1-\kappa_2}\big[-(\kappa_2-\omega)^2+2-\kappa_2-\omega\big]+(1\leftrightarrow 2)\\
&+\frac{L_2}{s-2-2\omega+\kappa_1+\kappa_2}\Big\{s^2(2\kappa_2-2)+s\big[2(\kappa_2-\omega)^2-6\kappa_2-2\omega+11\big]\\
&-2(\kappa_2-\omega)^2+4\kappa_2-8\omega-2\Big\}+(1\leftrightarrow 2),
\end{aligned}
$$

$$
\begin{aligned}
G^{(6)} =& \frac{18\omega}{\kappa_1-\kappa_2}(\kappa_2 L_2-\kappa_1 L_1)+\frac{s^2}{6}-\frac{s}{12}\big[6(\kappa_1+\kappa_2)+8\omega-40\big] \\
&-\big[\frac{1}{2}(\kappa_1+\kappa_2)-\omega\big]^2+\kappa_1+\kappa_2-\frac{3}{4}(\kappa_1-\kappa_2)^2+\frac{2}{3}\omega \\
&+\frac{L_2}{2+2\omega-\kappa_1-\kappa_2-s}\Big\{s^2(4\kappa_2-\kappa_2^2)+s\big[-2\kappa_2(\kappa_2-\omega)^2 \\
&+8\kappa_2^2-8\omega\kappa_2-9\kappa_2+4(\omega-2)(\omega-1)\big] \\
&-(\kappa_2-\omega)^4+4\kappa_2(\kappa_2-\omega)^2-5\kappa_2^2+(2\omega+2)\kappa_2+9\omega^2-8\omega\Big\}+(1\leftrightarrow 2),
\end{aligned}
$$

$$
\begin{aligned}
G^{(7)} =& \frac{L_2}{\kappa_1-\kappa_2}\big[s(\kappa_2-\omega-2)^2-4(\kappa_2-\omega)^2+8\kappa_2-28\omega-4\big]+(1\leftrightarrow 2) \\
&+\frac{L_2}{s-2-2\omega+\kappa_1+\kappa_2}\Big\{s^2(\omega-\kappa_2)+s\big[-(\kappa_2-\omega)^2+6(\kappa_2-\omega)\big] \\
&+4(\kappa_2-\omega)^2-8(\kappa_2+\omega)+4\Big\}+(1\leftrightarrow 2)+2s-8,
\end{aligned}
$$

$$
\begin{aligned}
G_i^{(8)} =& L_i\Big\{\kappa_i s^2(4+\omega-\kappa_i) \\
&+s\big[4\kappa_i^2-5(\kappa_i+3\omega)-(\kappa_i-\omega)^3-10\omega\kappa_i+6\omega^2+8\big] \\
&+2(\kappa_i-\omega)^3-8\omega(\kappa_i-\omega)-6\kappa_i-10\omega+4\Big\} \\
&+\frac{1}{6}\Big\{-s^3+s^2(3\kappa_i+\omega-18)+s\big[6(\kappa_i-\omega)^2-12\kappa_i+36\omega+28\big] \\
&-12(\kappa_i-\omega)^2-12\kappa_i+44\omega+24\Big\},
\end{aligned}
$$

$$
\begin{aligned}
G_i^{(9)} =& L_i\Big\{-\kappa_i s^2+s\big[\kappa_i-2+3\omega-(\kappa_i-\omega)^2\big]+4-2(\kappa_i+\omega)-2(\kappa_i-\omega)^2\Big\} \\
&+\frac{1}{4}\big[2s^2+4(\kappa_i-\omega-1)s+8(\kappa_i-\omega+2)\big],
\end{aligned}
$$

$$
G_i^{(10)} = s(1-s/2)+L_i\big[\frac{1}{2}(\kappa_i+\omega)s^2-s(2+\kappa_i+3\omega)+12\omega\big]. \qquad \text{(A9)}
$$

At zero velocity, the Higgs and Z exchange diagrams vanish, and only the chargino exchange diagrams remain. The rather lengthy expression for σ_{WW} times the relative velocity reduces to

$$
\sigma_{WW}v(v\to 0)=\frac{g^4(\omega-1)^{3/2}}{128\pi|m_{\tilde{\chi}}|m_W}\left[\frac{e_1^2+f_1^2}{1-\omega-\kappa_1}+\frac{e_2^2+f_2^2}{1-\omega-\kappa_2}\right]^2. \qquad \text{(A10)}
$$

In the early Universe, $v^2\approx 1/4$ at freeze-out and the v^2 terms are most certainly

of importance. However, in the galactic halo, neutralino-neutralino relative velocities are of order $v^2 = v_{\rm halo}^2 \approx 0$, and to a good approximation, the annihilation cross section times relative velocity should be given by $\sigma_{WW} v (v \to 0)$ (unless it vanishes).

APPENDIX B: CROSS SECTION FOR $\widetilde{\chi}\widetilde{\chi} \to Z^0 Z^0$

The matrix element for the process $\widetilde{\chi}\widetilde{\chi} \to Z^0 Z^0$ is given by the Feynman diagrams shown in Fig. 3, and the total cross section, averaged over the neutralino spins, is given by an analogous expression to that for σ_{WW}:

$$\sigma_{ZZ} = \frac{X_t}{64\pi s m_Z^2} \left(\frac{s-4}{s-4\omega} \right)^{\frac{1}{2}} \left(X_{HH} + X_{\widetilde{\chi}^0\widetilde{\chi}^0} + X_{H\widetilde{\chi}^0} \right). \tag{B1}$$

In this Appendix, it is most useful to rescale some quantities that have dimensions of mass by the mass of the Z. Specifically,

$$\omega = \left(\frac{m_{\tilde{\chi}}}{m_Z} \right)^2; \qquad \kappa_i = \left(\frac{m_{\tilde{\chi}_i^0}}{m_Z} \right)^2; \qquad s = \frac{(p_1+p_2)^2}{m_Z^2}, \tag{B2}$$

where $s m_Z^2$ is the square of the center of mass energy.

The quantity X_{HH} is given by

$$X_{HH} = \left(\frac{g^2 A'}{2 \sin\beta \cos\theta_W} \right)^2 \left[2 + (\frac{s}{2} - 1)^2 \right] (s - 4\omega), \tag{B3}$$

where A' is the same as in the W^+W^- case (Appendix A) except that here the Higgs masses in the denominators are divided by m_Z^2 instead of m_W^2. (The quantities A, C, Q, and R are still given by the same expressions in Appendix A.) Next, the quantities $X_{H\widetilde{\chi}^0}$ and $X_{\widetilde{\chi}^0\widetilde{\chi}^0}$:

$$\begin{aligned} X_{H\widetilde{\chi}^0} &= \frac{-g^4 A'}{4 \sin\beta \cos\theta_W} \sum_{i=1}^{4} C_i \left[\frac{m_{\tilde{\chi}}}{m_Z} G_i^{(9)} - \frac{m_{\tilde{\chi}_i^0}}{m_Z} G_i^{(10)} \right], \\ X_{\widetilde{\chi}^0\widetilde{\chi}^0} &= \frac{g^4}{16} \sum_{i,j=1}^{4} D_{ij} \left[G_{ij}^{(4)} - G_{ij}^{(6)} - (\frac{m_{\tilde{\chi}_i^0}}{m_Z} + \frac{m_{\tilde{\chi}_j^0}}{m_Z}) \frac{m_{\tilde{\chi}}}{m_Z} G_{ij}^{(5)} + \frac{m_{\tilde{\chi}_i^0}}{m_Z} \frac{m_{\tilde{\chi}_j^0}}{m_Z} G_{ij}^{(7)} \right], \end{aligned} \tag{B4}$$

where the sum is over the four neutralinos. Here the G_{ij}^k are given by the expressions in Appendix A with κ_1 and κ_2 being replaced by κ_i and κ_j (the L_i are

changed in the same way). The masses of all four neutralinos enter as they are virtual particles exchanged in the t- and u-channel diagrams.

The new quantities C_i and D_{ij} that appear above are defined by

$$C_i = 2e_i^2, \qquad D_{ij} = 2e_i^2 e_j^2, \tag{B5}$$

where the e_i are now given by

$$e_i = \frac{1}{\cos\theta_W}(Z_{i3}Z_{n3} - Z_{i4}Z_{n4}). \tag{B6}$$

For more discussion of the couplings see Refs. 1 and 11.

In the zero-velocity limit, the Higgs exchange diagrams again vanish, and only the chargino exchange diagrams are nonzero. In this limit

$$\sigma_{ZZ}v(v \to 0) = \frac{g^4(\omega-1)^{3/2}}{64\pi|m_{\tilde{\chi}}|m_Z}\left[\sum_{i=1}^{4}\frac{e_i^2}{1-\omega-\kappa_i}\right]^2. \tag{B7}$$

Once again, this formula is a good approximation for neutralino annihilation in the galactic halo, but is not applicable to relic abundance calculations.

APPENDIX C: CROSS SECTION FOR $\widetilde{\chi}\widetilde{\chi} \to H_i^0 H_j^0$

The total cross section for the process $\widetilde{\chi}\widetilde{\chi} \to H_i^0 H_j^0$ involves the Feynman diagrams of Figs. 4 and 5, and is given by

$$\sigma_{ij}v = \frac{g^4|\vec{k}|}{8\pi s|m_{\tilde{\chi}}|}\frac{X^{\rm tot}}{S}, \tag{C1}$$

where $|\vec{k}|$ is the magnitude of the outgoing momentum, $s = 4E^2 = 4m_{\tilde{\chi}}^2/(1-v^2/4)$ is the center of mass energy squared, and S is the symmetry factor (2 for $i = j$ and 1 otherwise). Note that in this Appendix, we have *not* rescaled any quantities by a particle mass.

The CP quantum number of the final state $\xi = c_i c_j$, where c_i is the CP quantum number of H_i^0 and $c_1 = c_2 = -c_3 = 1$, determines the form of $X^{\rm tot}$.

For $\xi = 1$ (see Fig. 4), $X^{\rm tot}$ is given by

$$X^{\rm tot} = 2p^2 \left[(B - 2U)^2 + \frac{2}{9}(4Ek^2V)^2 \right], \tag{C2}$$

where

$$\begin{aligned} U &= c_i \sum_{k=1}^{4} \frac{M_{ink} M_{jnk}}{t_0 - m^2_{\tilde{\chi}^0_k}} \left[m_{\tilde{\chi}} + c_i m_{\tilde{\chi}^0_k} + \frac{2 m_{\tilde{\chi}} k^2}{3(t_0 - m^2_{\tilde{\chi}^0_k})} \right], \\ V &= \sum_{k=1}^{4} \frac{M_{ink} M_{jnk}}{\left(t_0 - m^2_{\tilde{\chi}^0_k} \right)^2}, \qquad B = M_{1nn} H_{1ij} P_{H^0_1} + M_{2nn} H_{2ij} P_{H^0_2}, \\ P_{H^0_i} &= \left[(s - m^2_{H^0_i})^2 + m^2_{H^0_i} \Gamma^2_{H^0_i} \right]^{-1/2}, \end{aligned} \tag{C3}$$

and $\Gamma_{H^0_i}$ is the width of H^0_i. In this case, the contributions from the s-channel exchange of H^0_3 and Z vanish. Furthermore, $X^{\rm tot}$ vanishes at $v = 0$, so that $\sigma_{ij} v$ also vanishes as $v \to 0$.

For $\xi = -1$ (see Fig. 5), $X_{\rm tot}$ is given by

$$X^{\rm tot} = \frac{16}{3} p^2 k^2 (D + U)^2 + 2 \left[EC - \frac{m_{\tilde{\chi}} \delta D}{2E} \left(1 - \frac{s}{m^2_Z} \right) - 2V \right]^2, \tag{C4}$$

where

$$\begin{aligned} U &= c_i \sum_{k=1}^{4} \frac{M_{ink} M_{jnk}}{t_0 - m^2_{\tilde{\chi}^0_k}}, \\ V &= \sum_{k=1}^{4} \frac{M_{ink} M_{jnk}}{t_0 - m^2_{\tilde{\chi}^0_k}} \left[m_{\tilde{\chi}^0_k} E - \frac{c_i m_{\tilde{\chi}} \delta}{4E} \right] \left[1 + \frac{v^2}{4} \left(\frac{t_1^2}{3 \left(t_0 - m^2_{\tilde{\chi}^0_k} \right)^2} - \frac{t_2}{t_0 - m^2_{\tilde{\chi}^0_k}} \right) \right], \\ C &= M_{3nn} H_{3ij} P_{H^0_3}, \qquad D = \frac{F A_{ij}}{2 \cos\theta_W \left[(s - m^2_Z)^2 + m^2_Z \Gamma^2_Z \right]^{1/2}}, \end{aligned} \tag{C5}$$

and Γ_Z is the Z width. In this case, the contributions from s-channel exchange of H^0_1 and H^0_2 vanish.

The expressions given above contain terms of all orders in v^2; however, they are only correct to $\mathcal{O}(v^2)$. They are given this way for brevity. By evaluating these formulas at two small values of v, the coefficients of the leading order terms, a and b, may be obtained; here, $\sigma v = a + bv^2 + \cdots$.

The kinematic quantities used above are:

$$\begin{aligned} p &= |m_{\tilde{\chi}}|v/2, \\ k^2 = |\vec{k}|^2 &= \frac{s}{4} - \frac{1}{2}\left(m^2_{H^0_i} + m^2_{H^0_j}\right) + \frac{\delta^2}{4s}, \\ t_0 &= \frac{1}{2}\left(m^2_{H^0_i} + m^2_{H^0_j}\right) - m^2_{\tilde{\chi}}, \qquad t_1 = 2|m_{\tilde{\chi}}|k, \\ t_2 &= -2m^2_{\tilde{\chi}}, \qquad \delta = m^2_{H^0_i} - m^2_{H^0_j}. \end{aligned} \tag{C6}$$

The quantities A_{ij} are the $Z H^0_i H^0_j$ couplings:

$$A_{31} = -A_{13} = \frac{\sin(\alpha-\beta)}{2\cos\theta_W}; \qquad A_{32} = -A_{23} = \frac{\cos(\alpha-\beta)}{2\cos\theta_W}; \tag{C7}$$

and all other A_{ij} are zero. The quantities H_{ijk} are the $H^0_i H^0_j H^0_k$ couplings, and H_{ijk} is symmetric under the interchange of any two indices. The H_{ijk} are

$$\begin{aligned} H_{111} &= \frac{3m_Z}{2\cos\theta_W}\cos(\beta+\alpha)\cos 2\alpha, \\ H_{222} &= \frac{3m_Z}{2\cos\theta_W}\sin(\beta+\alpha)\cos 2\alpha, \\ H_{122} &= \frac{m_Z}{2\cos\theta_W}\left[2\sin(\beta+\alpha)\sin 2\alpha - \cos(\beta+\alpha)\cos 2\alpha\right], \\ H_{112} &= \frac{-m_Z}{2\cos\theta_W}\left[2\cos(\beta+\alpha)\sin 2\alpha + \sin(\beta+\alpha)\cos 2\alpha\right], \\ H_{133} &= \frac{-m_Z}{2\cos\theta_W}\cos(\beta+\alpha)\cos 2\beta, \\ H_{233} &= \frac{m_Z}{2\cos\theta_W}\sin(\beta+\alpha)\cos 2\beta, \\ H_{333} &= H_{113} = H_{123} = H_{223} = 0. \end{aligned} \tag{C8}$$

The quantities M_{kij} are the $H^0_k \chi^0_i \chi^0_j$ couplings, and M_{kij} is symmetric in the

indices i and j. The M_{kij} are

$$
\begin{aligned}
M_{1ij} &= \frac{-1}{2\sin\beta}\left[\frac{m_{\tilde{\chi}_i^0}\delta_{ij}\sin\alpha}{m_W} + 2(Q_{ij}\sin(\beta-\alpha) - R_{ij}\sin\alpha)\right], \\
M_{2ij} &= \frac{-1}{2\sin\beta}\left[\frac{m_{\tilde{\chi}_i^0}\delta_{ij}\cos\alpha}{m_W} - 2(Q_{ij}\cos(\beta-\alpha) + R_{ij}\cos\alpha)\right], \\
M_{3ij} &= \frac{-1}{2\sin\beta}\left[\frac{m_{\tilde{\chi}_i^0}\delta_{ij}\cos\beta}{m_W} - 2(Q_{ij}\cos 2\beta + R_{ij}\cos\beta)\right],
\end{aligned}
\tag{C9}
$$

where

$$
\begin{aligned}
Q_{ij} &= \frac{1}{2g}\left[Z_{i3}(gZ_{j2} - g'Z_{j1} + (i \leftrightarrow j)\right], \\
R_{ij} &= \frac{1}{2m_W}\left[MZ_{i2}Z_{j2} + M'Z_{i1}Z_{j1} - \mu(Z_{i3}Z_{j4} + Z_{i4}Z_{j3})\right].
\end{aligned}
\tag{C10}
$$

For further discussion of the couplings see Refs. 1 and 11.

In the limit $v \to 0$ the cross section becomes

$$
\begin{aligned}
\sigma_{ij}v(v\to 0) = &\frac{g^4|\vec{k}|}{16\pi|m_{\tilde{\chi}}|}\left[C - \frac{D\delta}{2m_{\tilde{\chi}}^2}\left(1 - \frac{4m_{\tilde{\chi}}^2}{m_Z^2}\right)\right. \\
&\left. - 2\sum_{k=1}^{4}\frac{M_{ink}M_{jnk}}{t_0 - m_{\tilde{\chi}_k^0}^2}\left(m_{\tilde{\chi}_k^0} - \frac{1}{4}c_i\delta/m_{\tilde{\chi}}\right)\right]^2.
\end{aligned}
\tag{C11}
$$

APPENDIX D: CROSS SECTION FOR $\tilde{\chi}\tilde{\chi} \to f\bar{f}$

The cross section for neutralino annihilation into quarks or leptons was found previously in Refs. 4 and 5, but we include here a slightly improved version. An error in the cross section given in Ref. 5 is corrected and Higgs exchange in the s-channel is included for the first time. The error involved the neglect of a part of the Z propagator and resulted in less than a 10% difference (ignoring Higgs exchange) when the cross section was used for annihilation in the early Universe ($v \approx 1/4$). However, as pointed out by Lars Bergstrom, it could be significant in the $v \to 0$ limit which is of relevance for halo annihilation. Higgs exchange is relatively unimportant for the heavy neutralino case discussed in this paper, but can make a difference for light neutralinos, especially near poles.[9]

To begin, we define the following

$$
\begin{aligned}
&a_q = m_q d_q/(2m_W), \qquad b_q = T_{3L} Z_{n2} - \tan\theta_W (T_{3L} - e_q) Z_{n1}, \\
&f_q = \tan\theta_W e_q Z_{n1}, \qquad F = Z_{n3}^2 - Z_{n4}^2. \\
&c_L = T_{3L} - e_q \sin^2\theta_W, \qquad c_R = -e_q \sin^2\theta_W, \\
&u_q' = a_q^2 + b_q^2, \qquad v_q' = a_q^2 + f_q^2, \qquad w_q' = a_q(b_q - f_q),
\end{aligned}
\tag{D1}
$$

Here $d_q = Z_{n3}/\cos\beta$ for down-type quarks or charged leptons and $d_q = Z_{n4}/\sin\beta$ for up-type quarks or neutral leptons, m_q is the mass of the fermion, T_{3L} is the weak isospin, and e_q is the fermion electric charge. Leaving out the Higgs exchange, the annihilation cross section, averaged over neutralino spins and to order v^2, is given by

$$
\begin{aligned}
\sigma_{f\bar{f}} v = \sum_q \frac{4}{\pi} G_F^2 c_q m_{\tilde{\chi}}^2 \beta' \Bigg\{ & y'^4 \Big[(u_q'^2 + v_q'^2)(z^2 + (a_1 + r_1)v^2) + 4w_q'^2 (1 + (a_2 + r_2)v^2) \\
& + 4w_q'(u_q' + v_q') z \big(1 + (\tfrac{1}{4}x^2 + r_3)v^2\big) + 2u_q' v_q' z^2 \big(1 + (a_4 + r_4)v^2\big) \Big] \\
& + F^2 x'^4 \Big[\frac{1}{4}(c_L^2 + c_R^2)(z^2 + a_1 v^2) + \frac{1}{2} c_L c_R z^2 (-1 - a_4 v^2) \Big] \\
& + F x'^2 y'^2 \Big[(v_q' c_R - u_q' c_L)(z^2 + (a_1 + z^2 r_5)v^2) \\
& + (u_q' c_R - v_q' c_L) z^2 \big(1 + (a_4 + r_5)v^2\big) - 2w_q'(c_L - c_R) z \big(1 + (\tfrac{1}{4}x^2 + r_5)v^2\big) \\
& \quad v^2 \beta'^2 r \Big(\frac{2}{3}(u_q' c_L - v_q' c_R) + w_q'(c_L - c_R) z \Big) \Big] \\
& + F^2 x'^4 \frac{(c_L - c_R)^2 z^2}{4} \frac{m_{\tilde{\chi}}^2}{m_Z^2} \left[\frac{16 m_{\tilde{\chi}}^2}{m_Z^2} - 8 + 2v^2 \left(\frac{2m_{\tilde{\chi}}^2}{m_Z^2}(1 + x^2) - x^2 \right) \right] \\
& + F(c_L - c_R) x'^2 y'^2 z \frac{m_X^2}{m_Z^2} \Big[2w_q' v^2 - \frac{4}{3} w_q' v^2 \beta'^2 r \\
& \quad + \left(2 + \frac{1}{2} v^2 (x^2 - 2r + \frac{4}{3}\beta'^2 r^2) \right) \left(4w_q' + 2z(u_q' + v_q') \right) \Big] \Bigg\}.
\end{aligned}
\tag{D2}
$$

The quantities a_i and r_i are given by

$$a_1 = \frac{2}{3} - \frac{5}{12}z^2 + \frac{1}{4}z^2x^2 \qquad a_2 = \frac{1}{4}(2 - z^2 + x^2)$$
$$a_4 = \frac{1}{4}(-3 + x^2) \qquad a_5 = 1 + x^2$$
$$r_1 = \frac{r}{3}(-4 + z^2 + 4r - 3rz^2 - rz^4) \qquad r_2 = \frac{r}{3}(-5 + 2z^2 + 3r\beta'^2 + 2rz^2\beta'^2)$$
$$r_3 = \frac{r}{3}(-3 + 5r\beta'^2 - 2\beta'^2) \qquad r_4 = \frac{r}{3}(-3 + 5r\beta'^2)$$
$$r_5 = \frac{r}{3}(-\frac{3}{2} + r\beta'^2) \qquad r_6 = \frac{r}{3}(-3 - \beta'^2 + 2r\beta'^2), \tag{D3}$$

where G_F is the Fermi constant, c_q is a color factor ($c_q = 3$ for quarks, $c_q = 1$ for leptons), $x'^2 = m_Z^2/((m_Z^2 - s)^2 + \Gamma_Z^2 m_Z^2)^{1/2}$ is the Z^0 pole factor, Γ_Z is the Z^0 width, $z = m_q/m_{\tilde{\chi}}$, $\beta' = (1 - z^2)^{1/2}$, and $y'^2 = m_W^2/(m_{\tilde{f}}^2 + \beta'^2 m_{\tilde{\chi}}^2)$ is the squark mass suppression including the propagator momentum. The propagator momenta factor $r = m_{\tilde{\chi}}^2/(m_{\tilde{f}}^2 + m_{\tilde{\chi}}^2\beta'^2)$ is usually small, as is $x^2 = \frac{1}{2}z^2/(1 - z^2)$. When $m_{\tilde{\chi}} \to m_q$ however, $z \to 1$, $x \to \infty$ and the expansion breaks down. However, this occurs only very close to mass thresholds and so these should be avoided. See Ref. 5 for the Feynman diagrams for $\tilde{\chi}\tilde{\chi} \to f\bar{f}$ and further discussion of the cross section.

Besides the squark and Z exchange diagrams included in Eq. (D2), there as s-channel diagrams involving the exchange of any of the three neutral Higgs

bosons. These contributions can be included by adding the following to Eq. (D2):

$$\sigma^H_{ff}v = \sum_q \frac{4G_F^2}{\pi} c_q m_{\tilde{\chi}}^2 \beta' \Big\{ (F_1+F_2)^2\beta'^2 v^2 + 4F_3^2(1+\frac{v^2}{4}a_5)$$
$$- 2FF_3 z(c_R-c_L)x'^2\left(1-\frac{4m_{\tilde{\chi}}^2}{m_Z^2}+\frac{v^2}{4}(x^2-\frac{4m_{\tilde{\chi}}^2}{m_Z^2}a_5)\right)$$
$$+ 2w'_q y'^2 v^2\left((F_1+F_2)\beta'^2(1-\frac{2r}{3})-F_3(a_5+2r_6)\right)$$
$$+ 2z(u'_q+v'_q)y'^2\left(\frac{1}{3}(F_1+F_2)r\beta'^2v^2-2F_3(1+v^2(r_5+\frac{x^2}{4}))\right)$$
$$- 8w'_q y'^2 F_3\Big\}, \tag{D4}$$

where $F_i = M_{inn}Q_{iq}m_W^2/((m_{H_i^0}^2-s)^2+m_{H_i^0}^2\Gamma_{H_i^0}^2)^{1/2}$, $\Gamma_{H_i^0}^2$ is the width of H_i^0, and

$$(Q_{1u},Q_{2u},Q_{3u}) = -\frac{m_q}{2m_W\sin\beta}(\sin\alpha,\cos\alpha,\cos\beta)$$
$$(Q_{1d},Q_{2d},Q_{3d}) = -\frac{m_q}{2m_W\cos\beta}(\cos\alpha,\sin\alpha,\sin\beta)\,. \tag{D5}$$

The quantities M_{knn}, Z_{ij}, $\tan\beta$, and $\sin\alpha$ were defined in Appendixes A and C.

In the limit $v \to 0$, relevant for present day neutralino annihilation, the annihilation total cross section (including Higgs exchange) reduces to

$$(\sigma_{ff}v)(v\to 0) = \sum_q \frac{4}{\pi}G_F^2 c_q m_{\tilde{\chi}}^2\beta'\Big[-2F_3+y'^2\left(2w'+z(u'+v')\right)$$
$$+\frac{x'^2}{2}F(c_R-c_L)z\left(1-4\frac{m_{\tilde{\chi}}^2}{m_Z^2}\right)\Big]^2. \tag{D6}$$

For further discussion of the couplings and the supersymmetric model, see Appendix A and Refs. 1, 5 and 11.

REFERENCES

1. H. E. Haber and G. L. Kane, *Phys. Rep.* **117**, 75 (1985).
2. For recent reviews of dark matter and its detection, see V. Trimble, *Ann. Rev. Astron. Astrophys.* **25**, 425 (1989); J. R. Primack, B. Sadoulet, and D. Seckel, *Ann. Rev. Nucl. Part. Sci.* **B38**, 751 (1988); *Dark Matter in the Universe*, eds. J. Kormendy and G. Knapp (Reidel, Dordrecht, 1989).
3. Since its mass is much greater than 1 keV, the LSP behaves as "cold" dark matter—dark matter with a small velocity dispersion—and based simply upon the equivalence principle, LSP dark matter should find its way into galactic halos. On the other hand, "hot" dark matter—a thermal relic much lighter than 1 keV—is not likely to find its way into galactic halos because of its large velocity dispersion. For further discussion, see Ref. 2.
4. J. Ellis, J. S. Hagelin, D. V. Nanopoulos, K. A. Olive, and M. Srednicki, *Nucl. Phys.* **B238**, 453 (1984).
5. K. Griest, *Phys. Rev.* **D38**, 2357 (1988); *Phys. Rev. Lett.* **61**, 666 (1988).
6. Olive and Srednicki have also addressed the possibility of neutralino dark matter heavier than the W mass; see K. A. Olive and M. Srednicki, University of Minnesota preprint UMN-TH-801/89 (1989). They do not treat the general neutralino state; rather, they treat the limiting cases of a gaugino-like and Higgsino-like neutralino, but arrive at similar conclusions.
7. K. Enqvist, K. Kainulainen, and J. Maalampi, *Nucl. Phys.* **B317**, 647 (1989).
8. R. A. Barbieri and G. F. Giudice, *Nucl. Phys.* **B306**, 63 (1988).
9. K. Griest and M. Kamionkowski, in preparation.
10. There is actually another mass parameter, M', but we adopt the usual simplification and set $M' = \frac{5}{3} M \tan^2 \theta_W$; see Ref. 1. Also, note that in Ref. 1, the parameter $\tan \theta_v = 1/\tan \beta$ is used in place of $\tan \beta$.
11. J. F. Gunion and H. E. Haber, *Nucl. Phys.* **B272**, 1 (1986).
12. J. F. Gunion and H. E. Haber, *Nucl. Phys.* **B278**, 449 (1986).

13. H. Goldberg, *Phys. Rev. Lett.* **50**, 1419 (1983).

14. L. Bergstrom, *Phys. Lett.* **B225**, 372 (1983); R. Flores, K. A. Olive, and S. Rudaz, University of Minnesota preprint UMN-TH-806/89 (1989).

15. E. W. Kolb and M. S. Turner, *The Early Universe* (Addison-Wesley, Redwood City, 1989).

16. F. Abe *et al.* (CDF collaboration), *Phys. Rev. Lett.*, in press (1989).

17. U. Amaldi *et al.*, *Phys. Rev.* **D36**, 1385 (1987); B. W. Lynn, M. E. Peskin, and R. G. Stewart, in *Physics at LEP*, CERN report CERN 86-02 (1986). The Almaldi *et al.* top quark mass limit is for the Standard Model, but Lynn *et al.* show that the corrections due to heavy squarks or sleptons go in the same direction as corrections due to a heavy top quark, and so the mass limit should not be weaker for the supersymmetric models we consider.

18. G. F. Giudice and G. Ridolfi, *Z. Phys.* **C41**, 447 (1988).

19. For a recent review and discussion of both direct and indirect detection, see, *e.g.*, J. Primack *et al.* in Ref. 2.

20. K. Griest and B. Sadoulet, in Proceeding of the Second Particle Astrophysics School on Dark Matter, Erice, Italy, 1988.

21. R. M. Barnett and H. E. Haber, *Phys. Rev.* **D31**, 85 (1985).

FIGURE CAPTIONS

1. Lightest neutralino composition and mass for $\tan\beta = 2$. The broken curves are contours of constant neutralino mass $m_{\tilde{\chi}}$, and the solid curves are contours of constant gaugino fraction $(Z_{n1}^2 + Z_{n2}^2)$; in (a) $\mu > 0$ and in (b) $\mu < 0$.

2. Feynman diagrams for neutralino annihilation into W^+W^- final states.

3. Feynman diagrams for neutralino annihilation into ZZ final states. The index i runs from 1 to 4.

4. Feynman diagrams for neutralino annihilation into $H_i^0 H_j^0$ final states where $c_i = c_j$. There are a total of ten diagrams since the index k runs from 1 to 4.

5. Feynman diagrams for neutralino annihilation into $H_i^0 H_j^0$ final states where $c_i \neq c_j$ ($H_2^0 H_3^0$ and $H_1^0 H_3^0$ only). The index k runs from 1 to 4.

6. Hatch plots that illustrate the importance of the various channels for neutralino annihilation in the early Universe ($v^2 \approx 1/4$). In the areas "hatched" with positively sloped lines, annihilation into fermion final states dominates by at least a factor of 10; in the regions marked by negatively sloped lines, annihilation into gauge-boson final states dominates by at least a factor of 10; and in the regions hatched with horizontal lines, annihilation into Higgs-boson final states dominates by at least a factor of 10. In the regions hatched by vertical lines, several final states contribute comparably to the annihilation. Here $m_{\tilde{f}} = m_{\tilde{\chi}}$ is used throughout. The values of m_t and $\tan\beta$, and the sign of μ are as indicated. Hatch plots for other values of m_t and $\tan\beta$ are qualitatively similar.

7. Same as Fig. 6(a) but with $m_{\tilde{f}} = 2m_{\tilde{\chi}}$.

8. Same as Fig. 6(a) but with $m_{\tilde{f}} = \infty$.

9. Relic neutralino abundance as a function of M for several fixed values of μ. The solid curves show $\Omega_{\tilde{\chi}} h^2$ assuming $m_{\tilde{f}} = m_{\tilde{\chi}}$, and the broken curves show $\Omega_{\tilde{\chi}} h^2$ assuming $m_{\tilde{f}} = \infty$. Here we have taken $\tan\beta = 2$ and $m_t = 60$

GeV. Results for $\mu < 0$ and other values of $\tan\beta$ and m_t are qualitatively similar.

10. Relic neutralino abundance as a function of μ for several fixed values of M. Again the solid curves show $\Omega_{\tilde{\chi}}h^2$ assuming $m_{\tilde{f}} = m_{\tilde{\chi}}$, and the broken curves show $\Omega_{\tilde{\chi}}h^2$ assuming $m_{\tilde{f}} = \infty$ for the same three values of M. Again we have taken $\tan\beta = 2$ and $m_t = 60$ GeV. Results for $\mu < 0$ and other values of $\tan\beta$ and m_t are qualitatively similar.

11. Relic neutralino abundance as a function of M for $\mu = \frac{5}{3}M\tan^2\theta_W$, $\tan\beta = 2$ and $m_t = 60$ GeV. Again the solid line shows $\Omega_{\tilde{\chi}}h^2$ assuming $m_{\tilde{f}} = m_{\tilde{\chi}}$, and the broken line shows $\Omega_{\tilde{\chi}}h^2$ assuming $m_{\tilde{f}} = \infty$. Again we have taken $\tan\beta = 2$ and $m_t = 60$ GeV. Plots for $\mu < 0$ and other values of $\tan\beta$ and m_t are similar.

12. Cosmologically excluded regions of the M-μ plane for several values of m_t using $\tan\beta = 2$. The hatched areas are those for which $\Omega_{\tilde{\chi}}h^2 > 1$ *independent* of $m_{H_2^0}$ and $m_{\tilde{f}}$. Plots for $\mu < 0$ and other values of $\tan\beta$ are very similar.

13. Same as Fig. 12(a) but assuming $m_{\tilde{f}} = \infty$.

14. Cosmological upper bound to $m_{\tilde{\chi}}$ as a function of $\tan\beta$ for several values of the top quark mass.

15. Scatter plots of $\Omega_{\tilde{\chi}}h^2$ vs. neutralino mass for a wide range of models (assuming $m_{\tilde{f}} = m_{\tilde{\chi}}$ and $\tan\beta = 2$). In (a) we use $m_t = 60$ GeV, and in (b) we use $m_t = 180$ GeV. Each "×" represents a different supersymmetric model specified by the value of μ and M. The values selected for M and μ were taken from a grid on the M-μ plane. Results for other values of $\tan\beta$ are qualitatively similar.

16. Same as Fig. 15(a) with $m_{\tilde{f}} = 2m_{\tilde{\chi}}$.

17. Same as Fig. 15(a) with $m_{\tilde{f}} = \infty$.

18. Scatter plot of estimated halo annihilation rate vs. neutralino mass for a wide range of models (assuming $m_{H_2^0} = 0$, $\tan\beta = 2$, $m_t = 60$, and using $m_{\tilde{f}} = m_{\tilde{\chi}}$ or $m_{\tilde{f}} = \infty$).

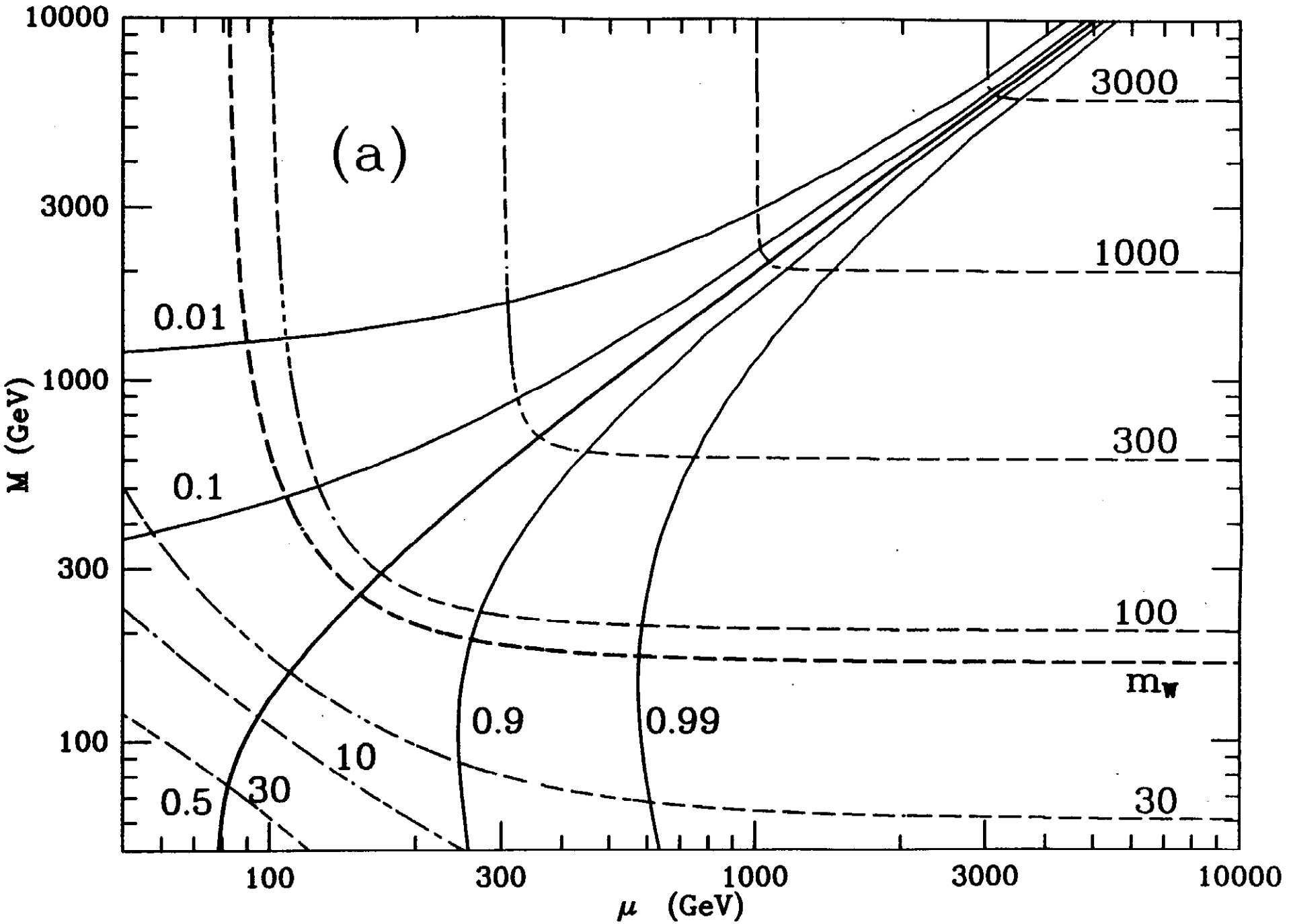
(a)
10000
3000
1000
300
100
M (GeV)
100
300
1000
3000
10000
μ (GeV)
0.01
0.1
0.5
30
10
0.9
0.99
3000
1000
300
100
m_W
30

Fig. 1(a)

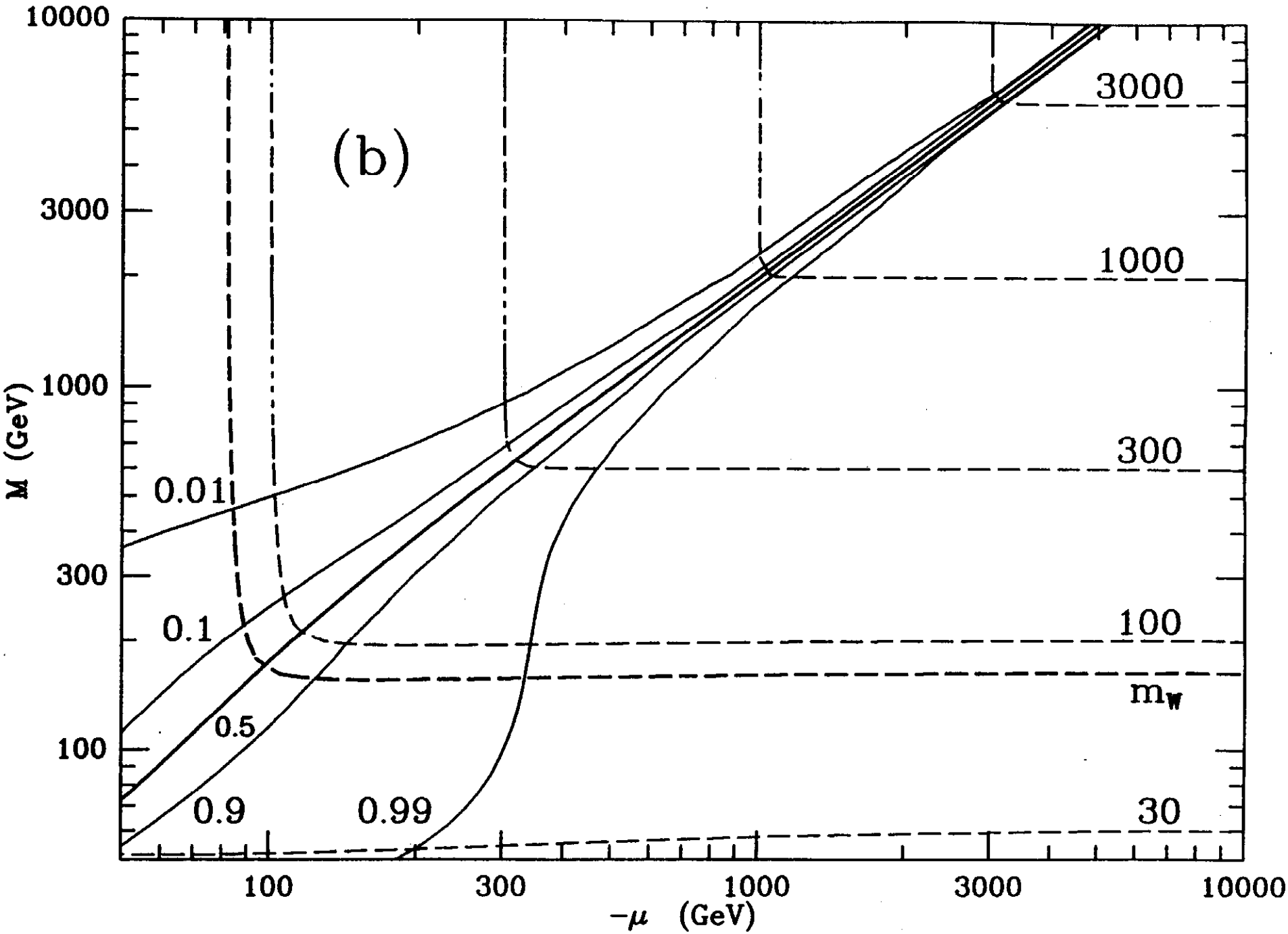
(b)
10000
3000
1000
300
100
M (GeV)
3000
1000
300
100
30
m_W
0.01
0.1
0.5
0.9
0.99
100
300
1000
3000
10000
$-\mu$ (GeV)

Fig. 1(b)

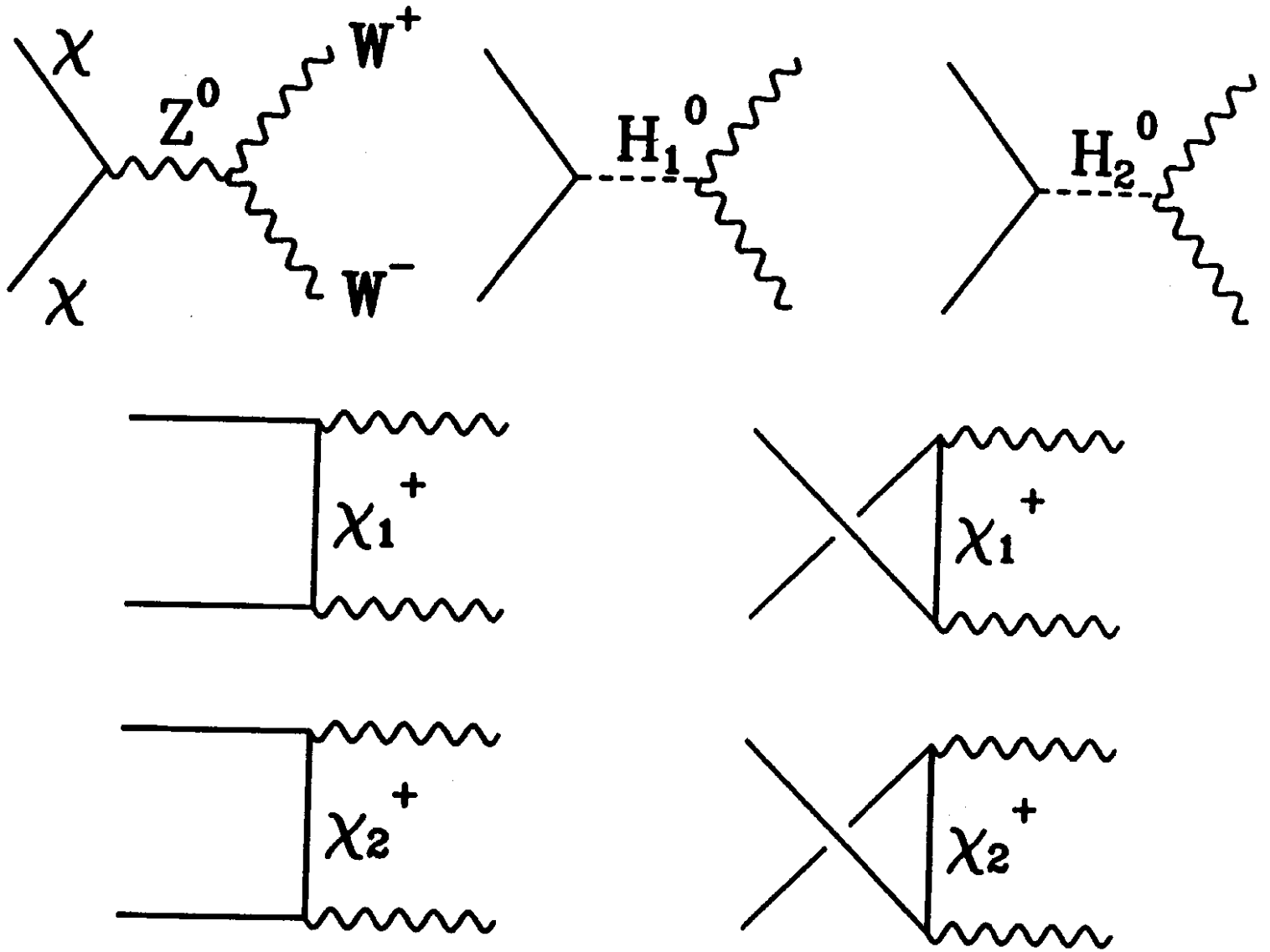

Fig. 2

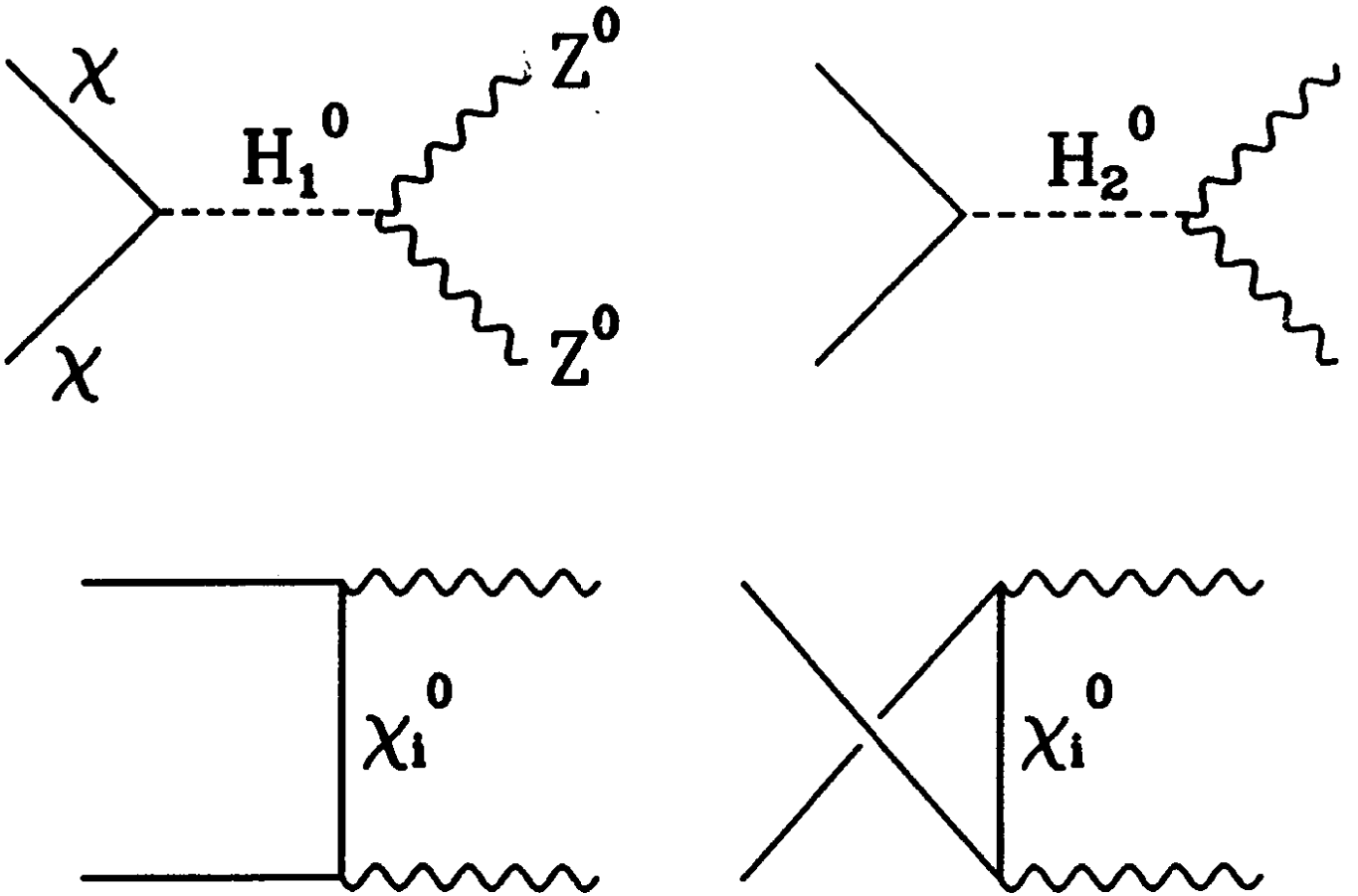

Fig. 3

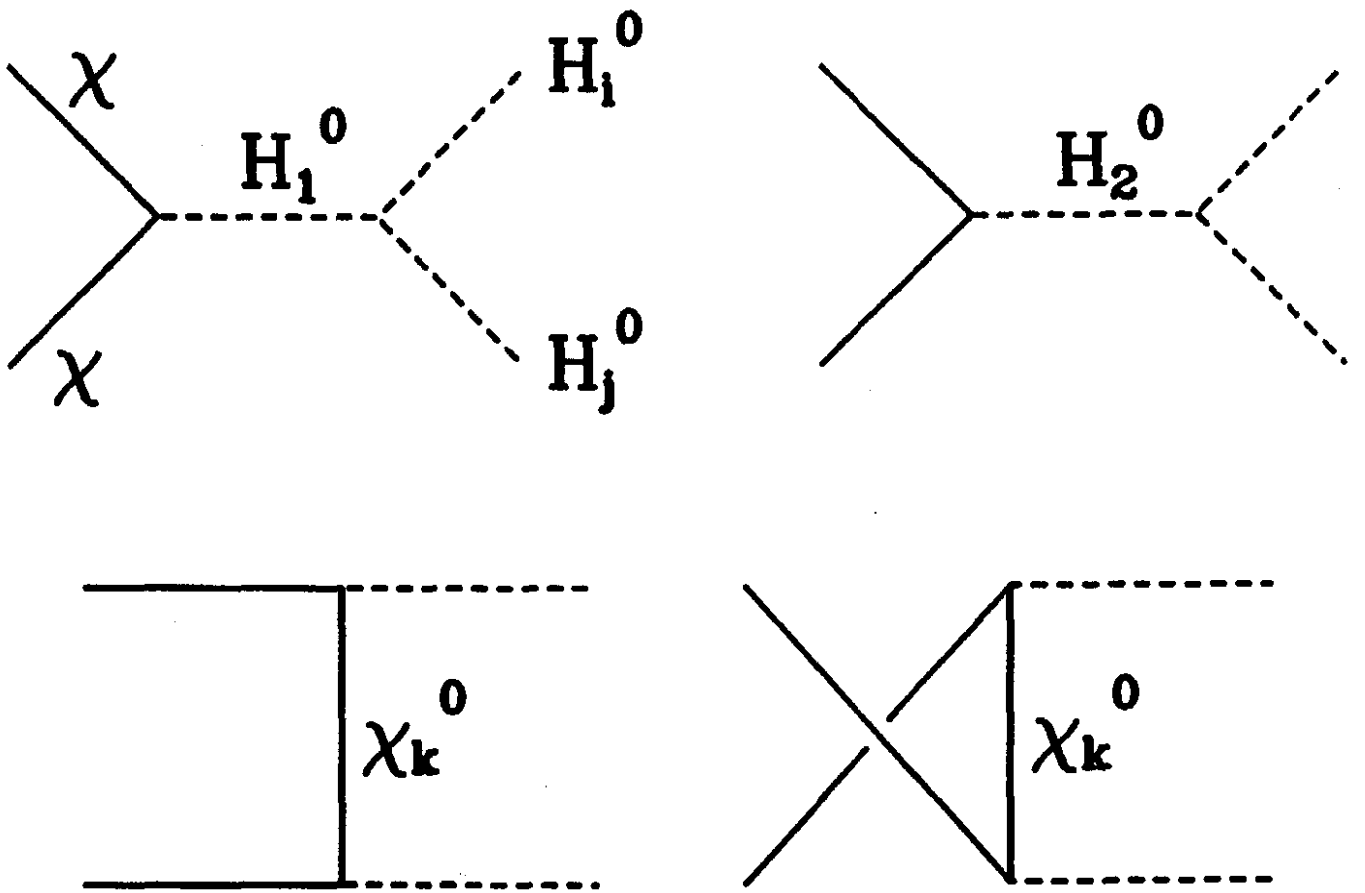

Fig. 4

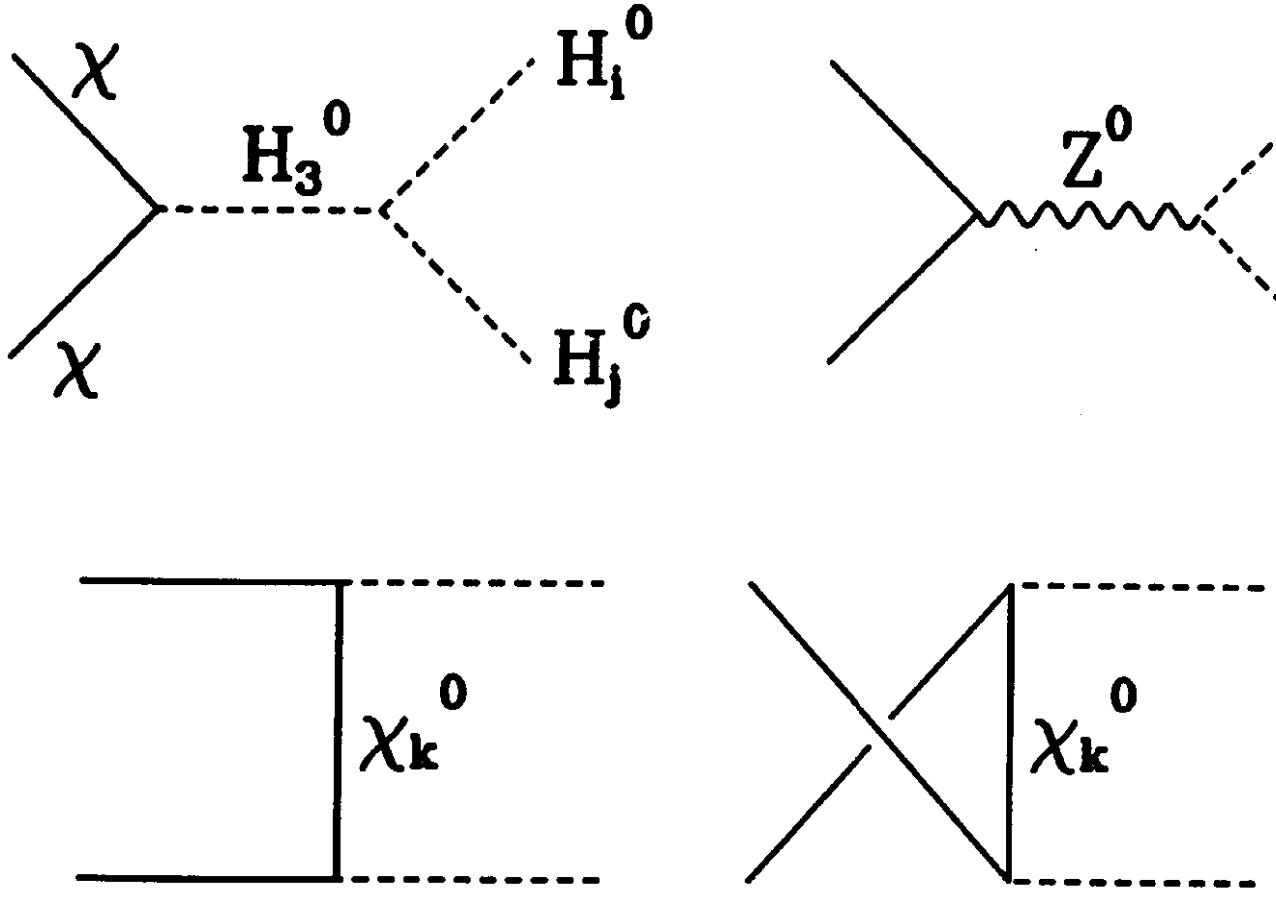

Fig. 5

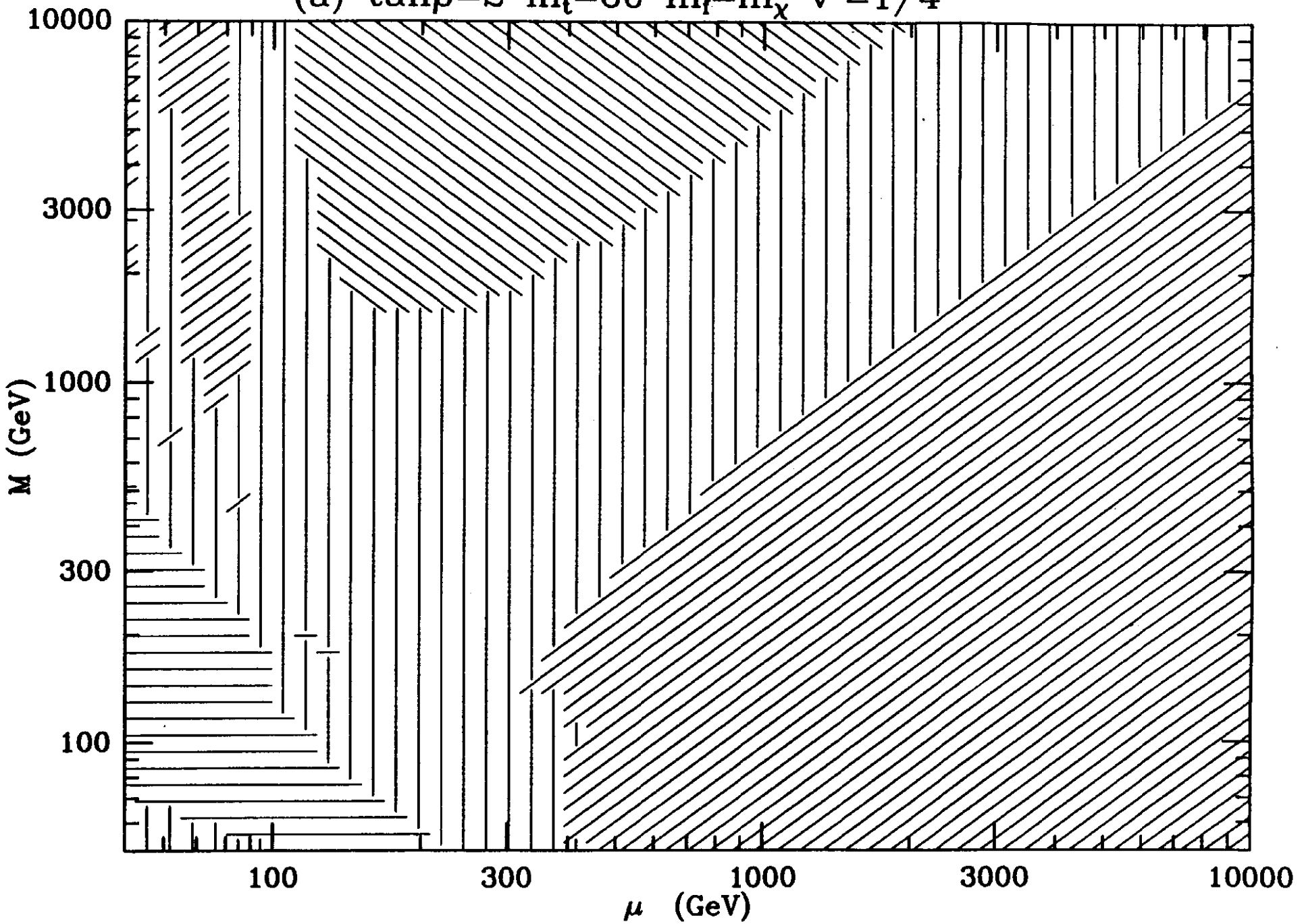
(a) tanβ=2 m_t=60 m_f=m_χ v^c=1/4
10000
3000
1000
300
100
M (GeV)
100
300
1000
3000
10000
μ (GeV)

Fig. 6(a)

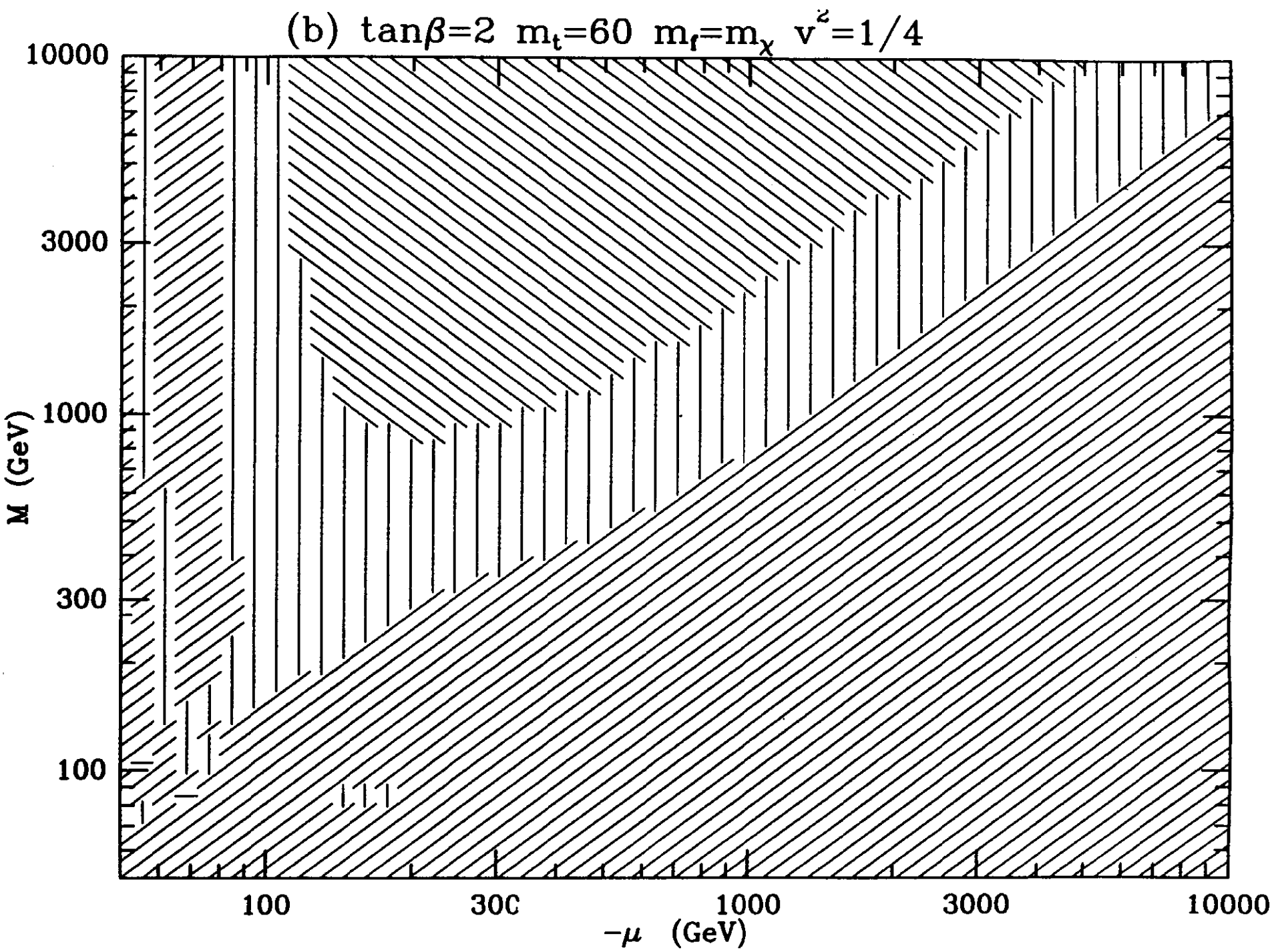
(b) tanβ=2 m_t=60 m_f=m_χ v^2=1/4
10000
3000
1000
300
100
M (GeV)
100
300
1000
3000
10000
−μ (GeV)

Fig. 6(b)

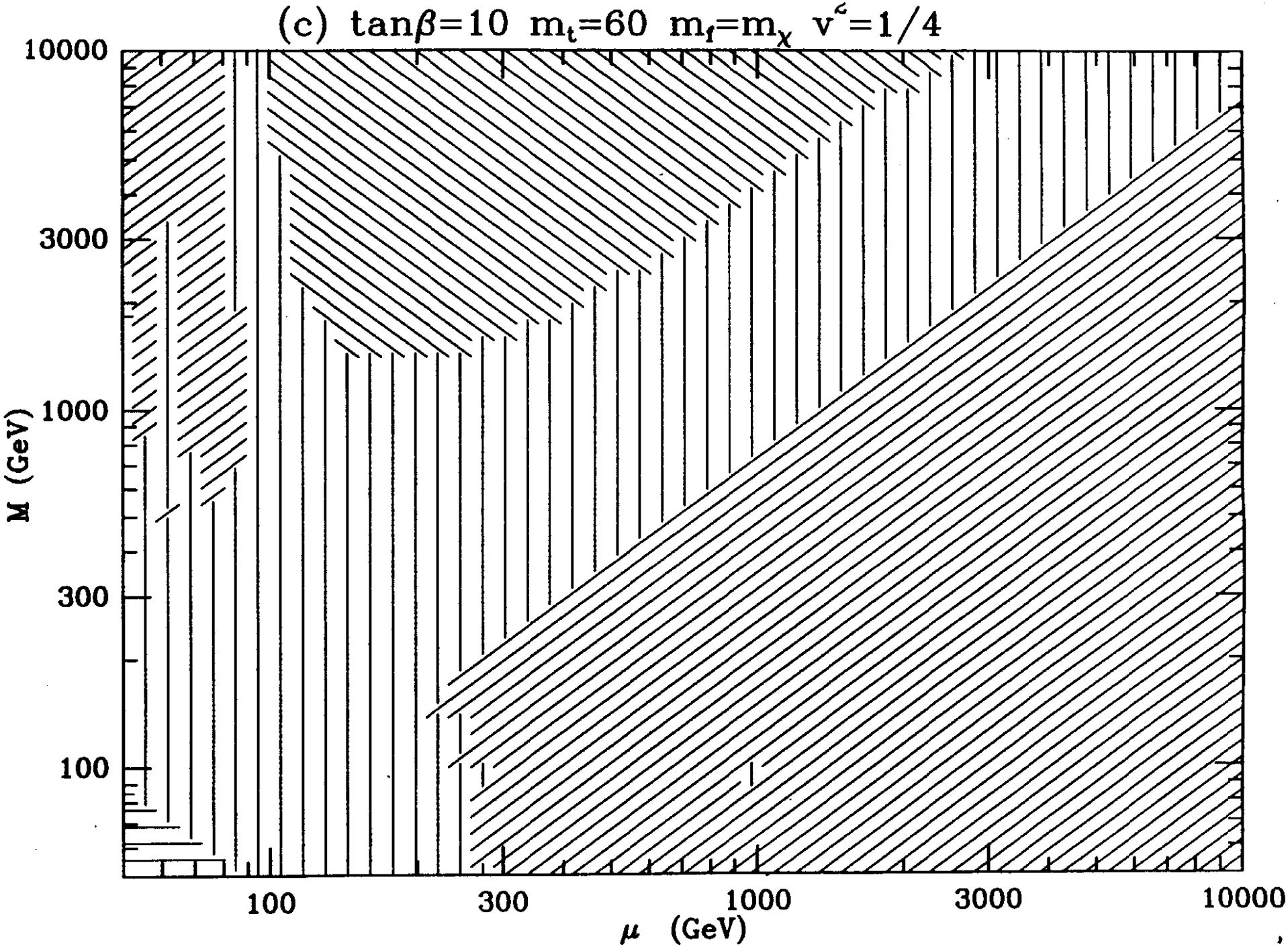
(c) tanβ=10 m_t=60 m_f=m_χ v^c=1/4
10000
3000
1000
300
100
M (GeV)
100
300
1000
3000
10000
μ (GeV)

Fig. 6(c)

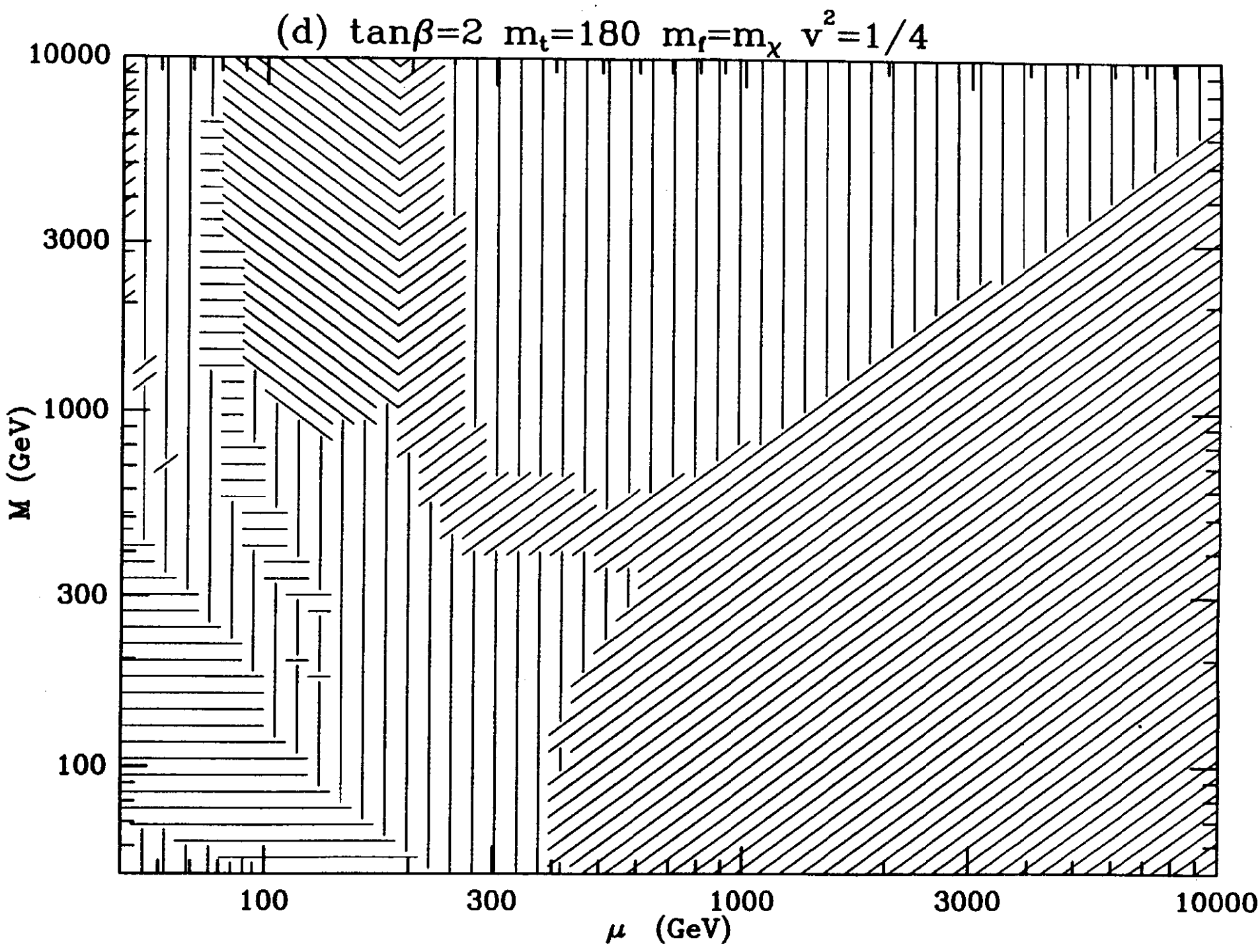
(d) tanβ=2 m_t=180 m_f=m_χ v²=1/4
10000
3000
1000
300
100
M (GeV)
100
300
1000
3000
10000
μ (GeV)

Fig. 6(d)

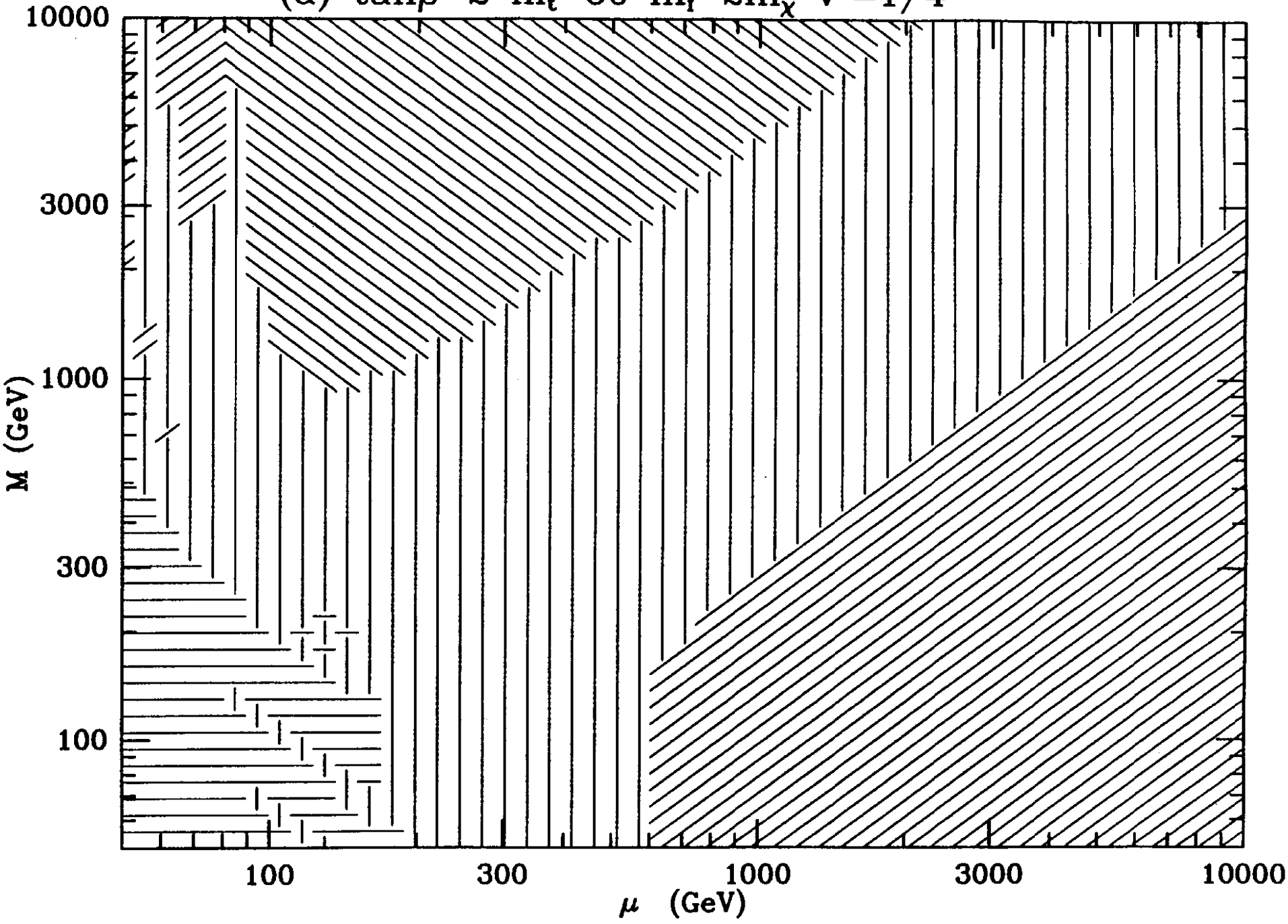
(a) tanβ=2 m_t=60 m_f=2m_χ v^2=1/4
10000
3000
1000
300
100
M (GeV)
100
300
1000
3000
10000
μ (GeV)

Fig. 7(a)

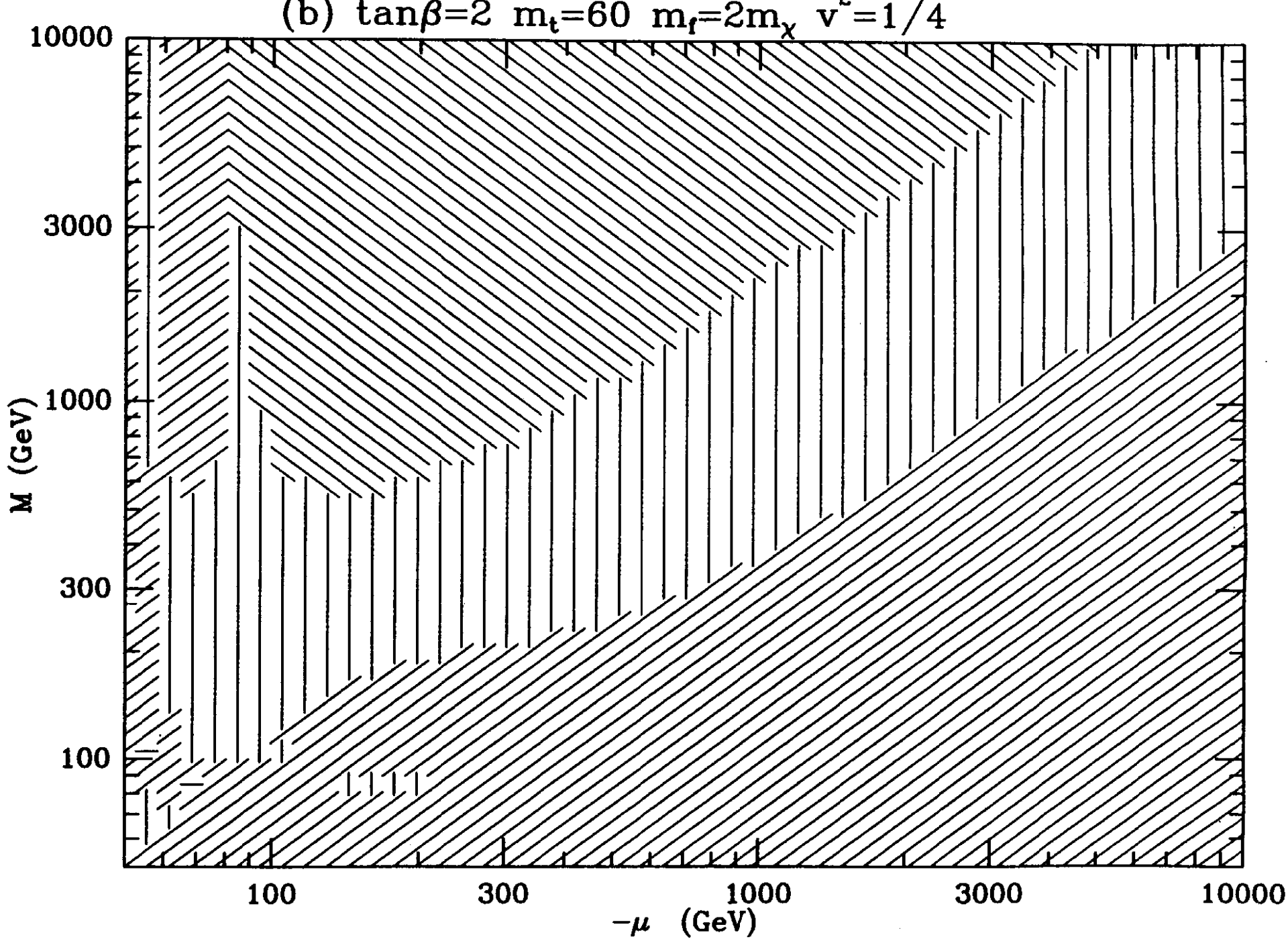
(b) tanβ=2 m_t=60 m_f=2m_χ v^2=1/4
10000
3000
1000
300
100
M (GeV)
100
300
1000
3000
10000
−μ (GeV)

Fig. 7(b)

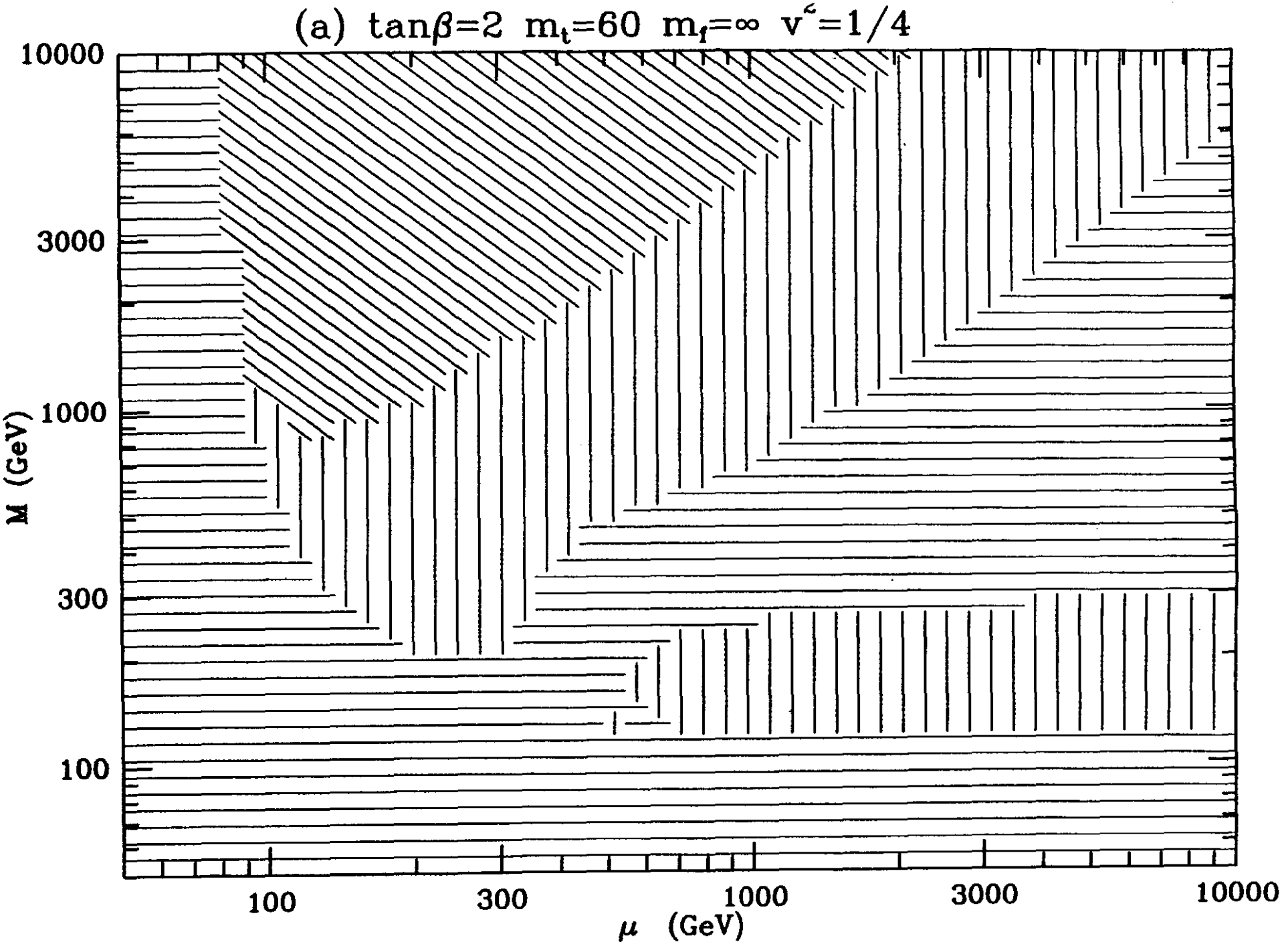
(a) tanβ=2 m_t=60 m_f=∞ v^c=1/4
10000
3000
1000
300
100
M (GeV)
100
300
1000
3000
10000
μ (GeV)

Fig. 8(a)

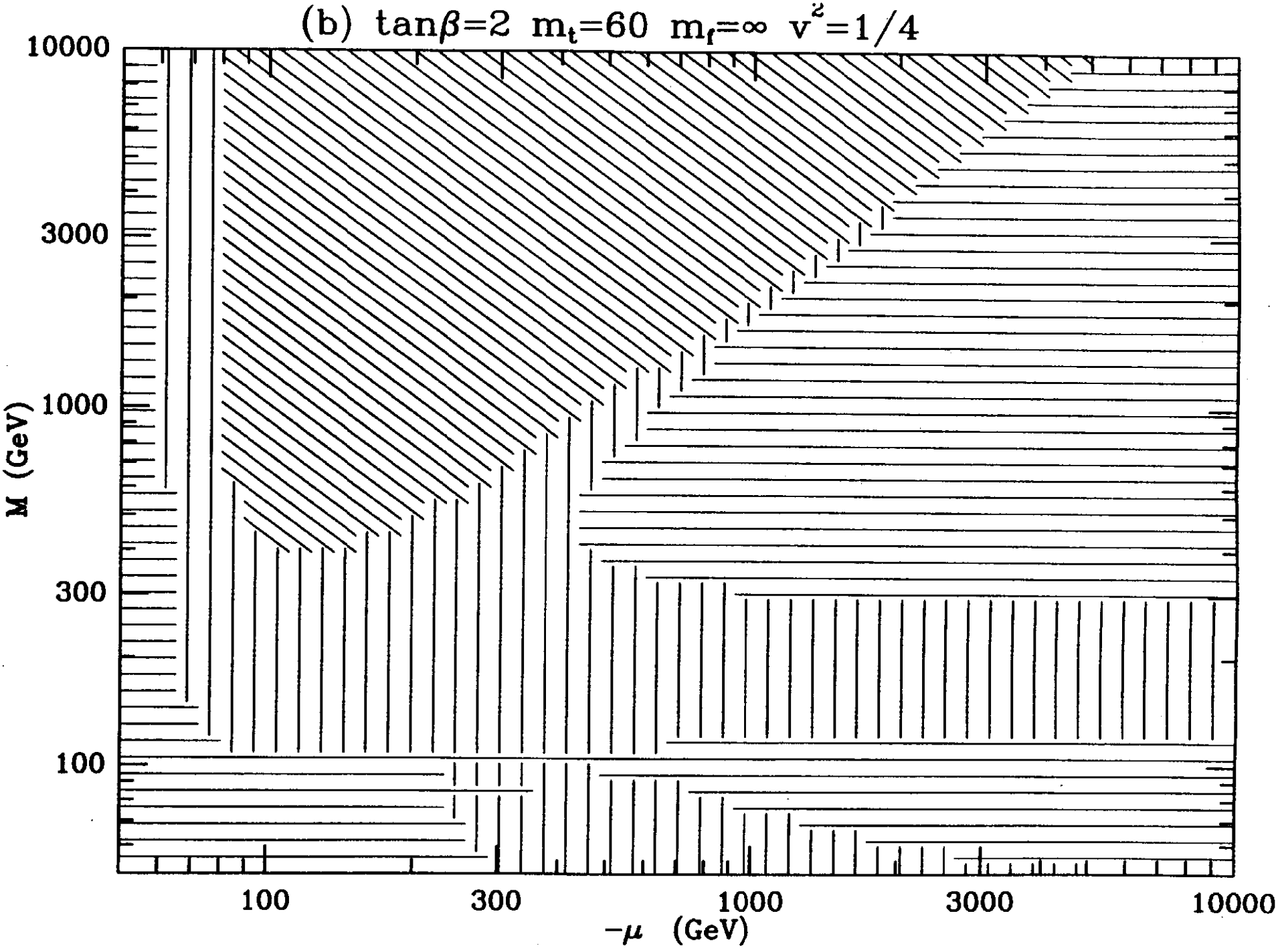
(b) tanβ=2 m_t=60 m_f=∞ v²=1/4
10000
3000
1000
300
100
M (GeV)
100
300
1000
3000
10000
−μ (GeV)

Fig. 8(6)

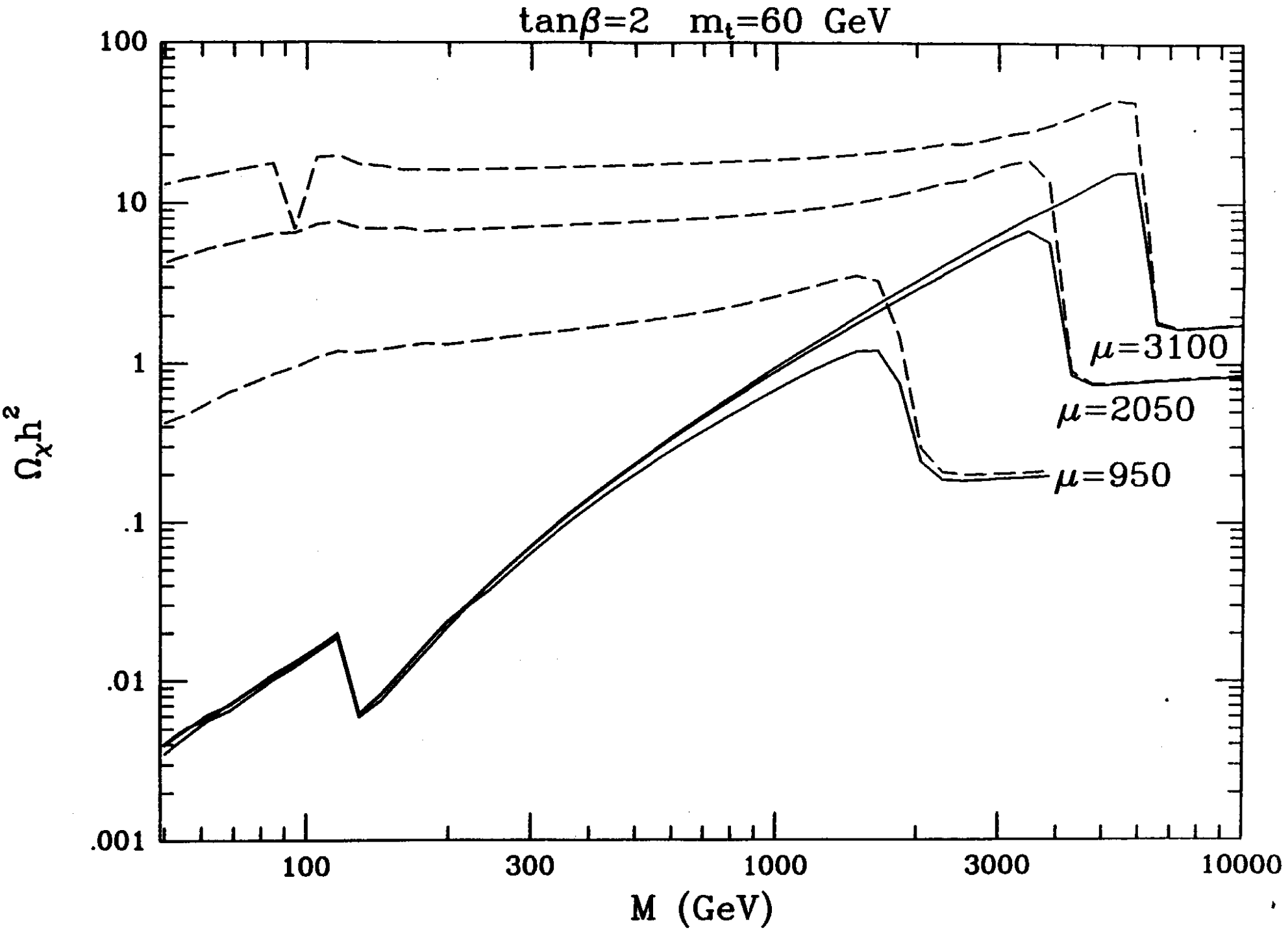
tanβ=2 m_t=60 GeV
100
10
1
.1
.01
.001
Ω_χh^2
100
300
1000
3000
10000
M (GeV)
μ=3100
μ=2050
μ=950

Fig. 9

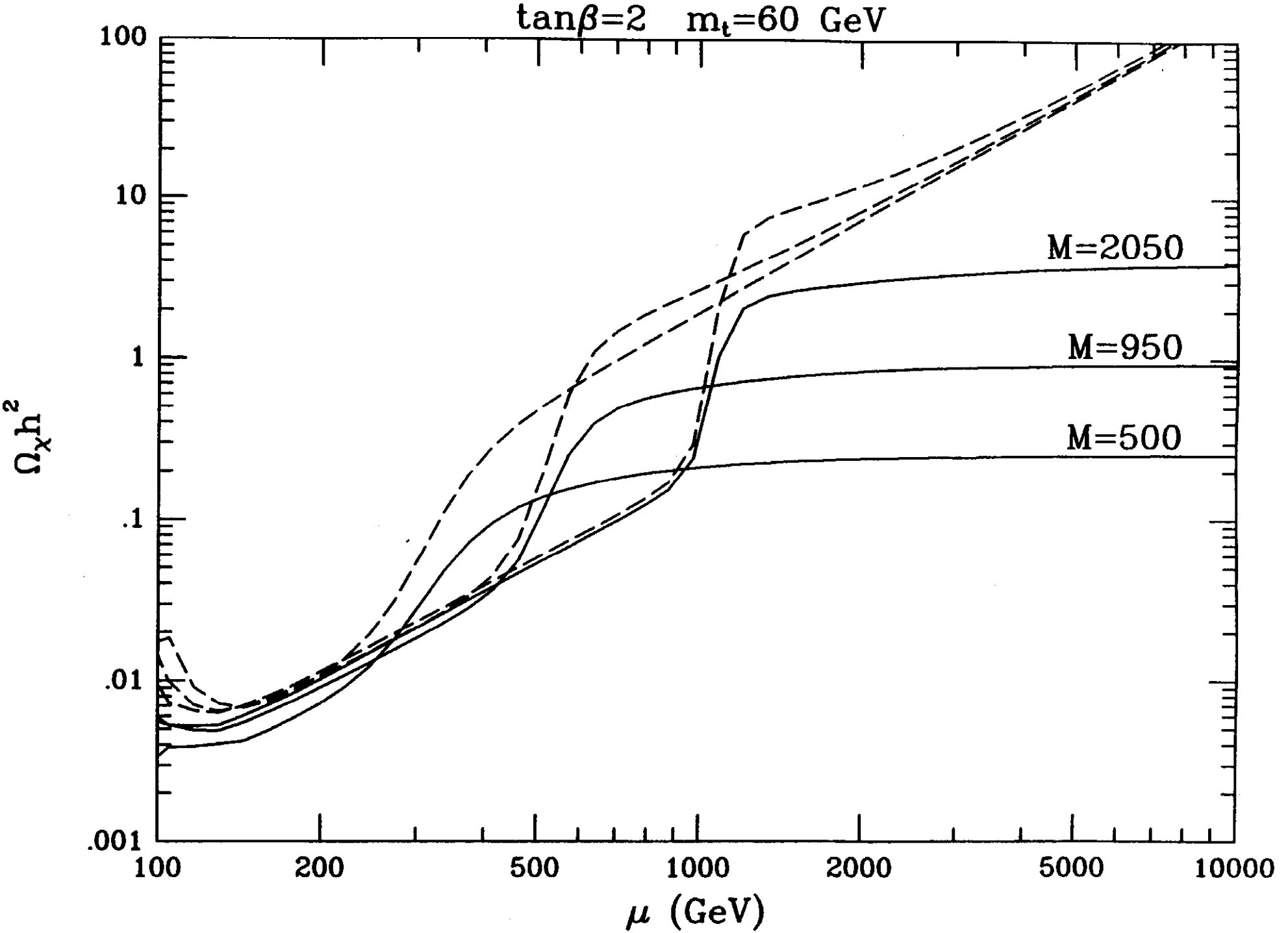
tanβ=2 m_t=60 GeV
100
10
1
.1
.01
.001
Ω_χh^2
M=2050
M=950
M=500
100
200
500
1000
2000
5000
10000
μ (GeV)

Fig. 10

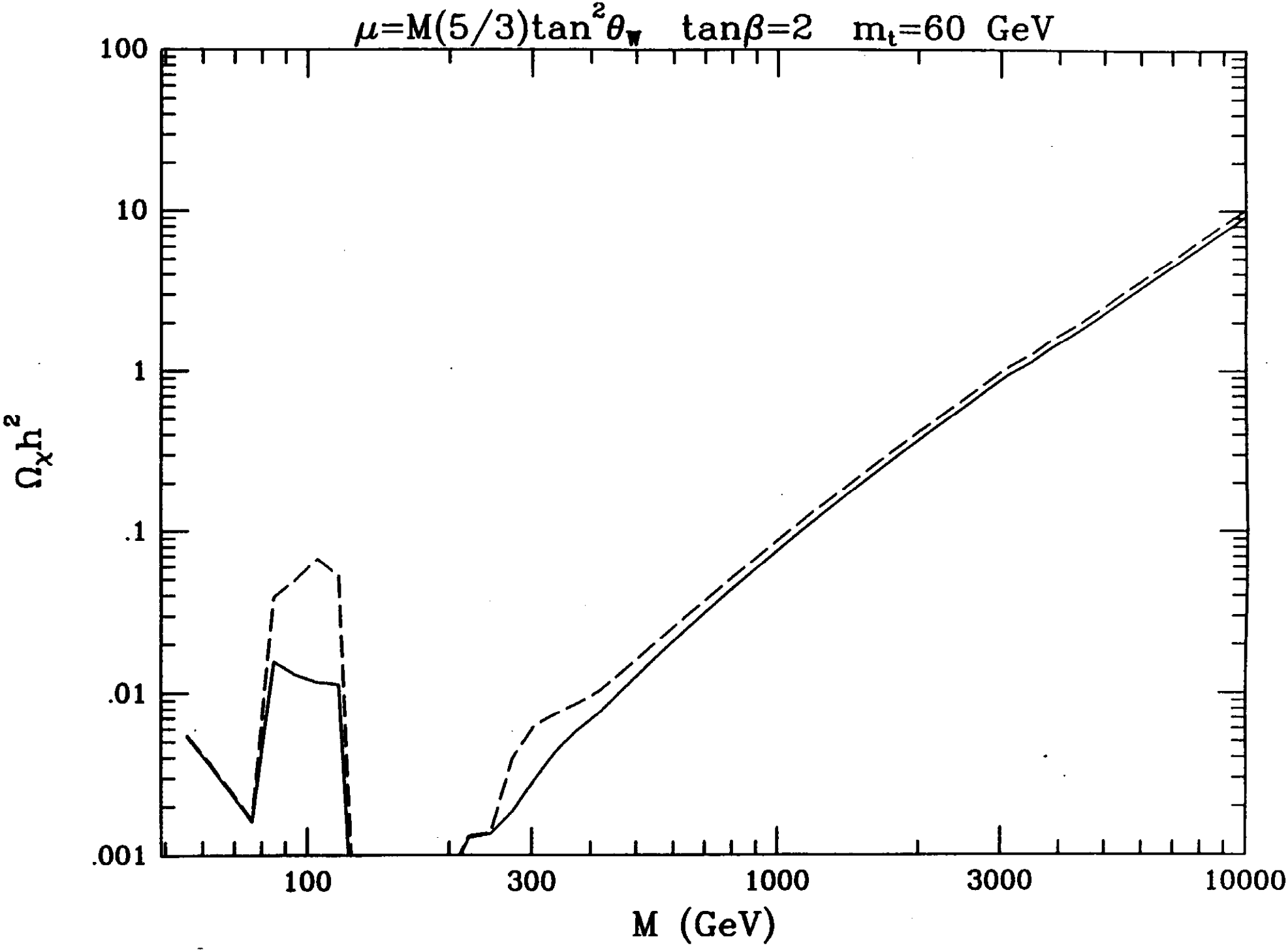
μ=M(5/3)tan$^2\theta_W$ tanβ=2 m_t=60 GeV
100
10
1
.1
.01
.001
$\Omega_\chi h^2$
100
300
1000
3000
10000
M (GeV)

Fig. 11

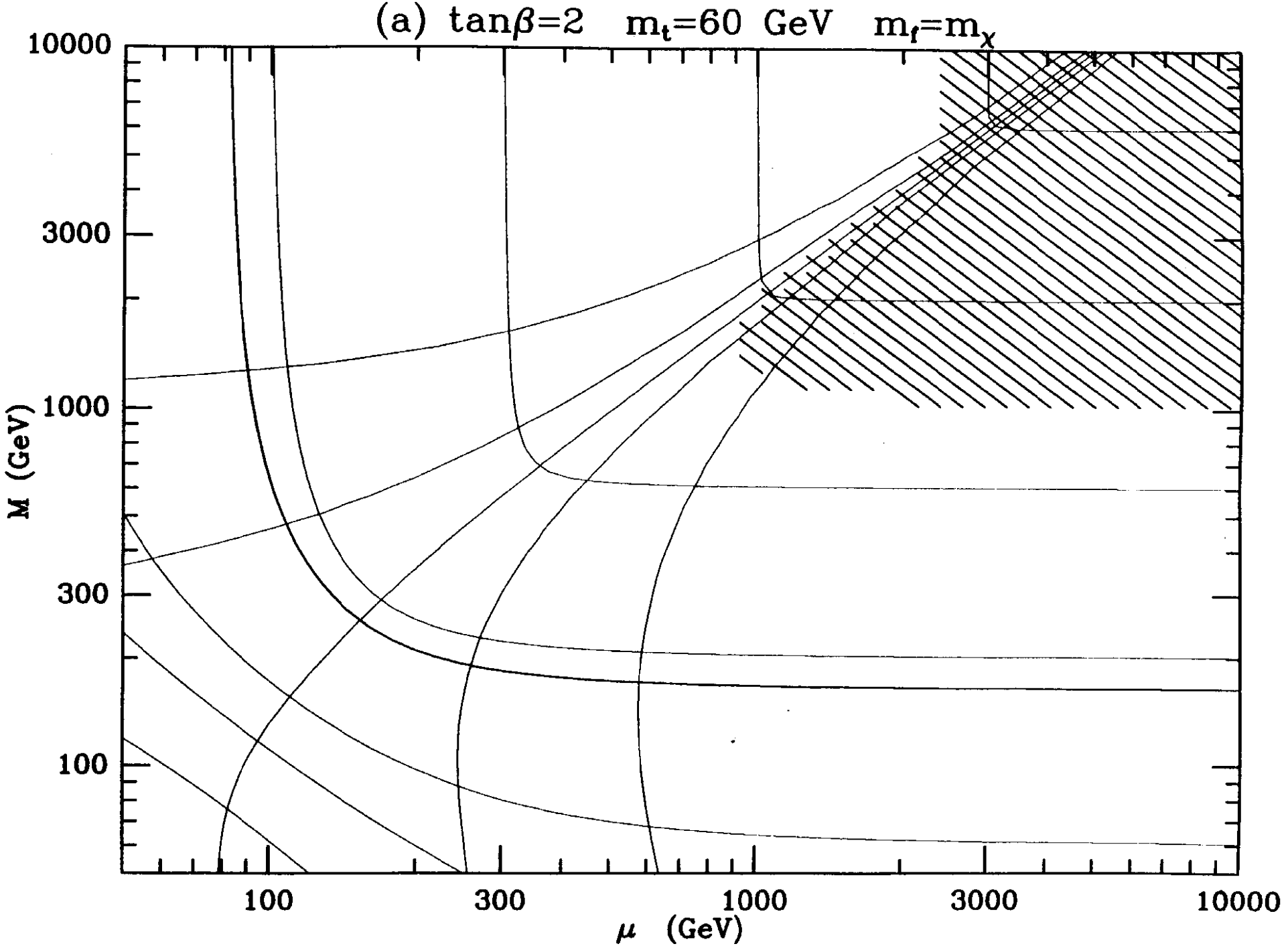
(a) tanβ=2 m_t=60 GeV m_f=m_χ
10000
3000
1000
300
100
M (GeV)
100
300
1000
3000
10000
μ (GeV)

Fig. 12(a)

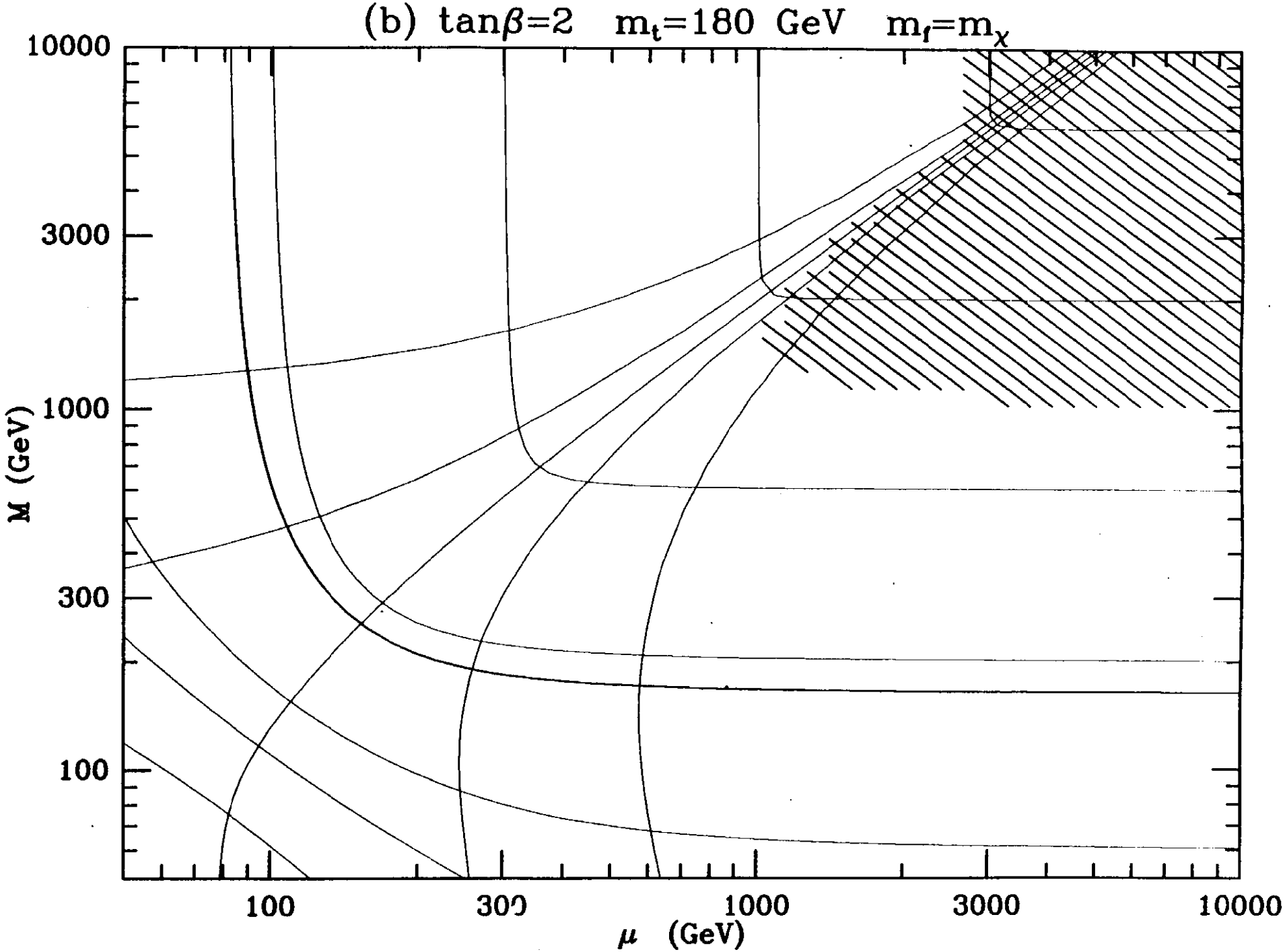
(b) tanβ=2 m_t=180 GeV m_f=m_χ
10000
3000
1000
300
100
M (GeV)
100
300
1000
3000
10000
μ (GeV)

Fig. 12(b)

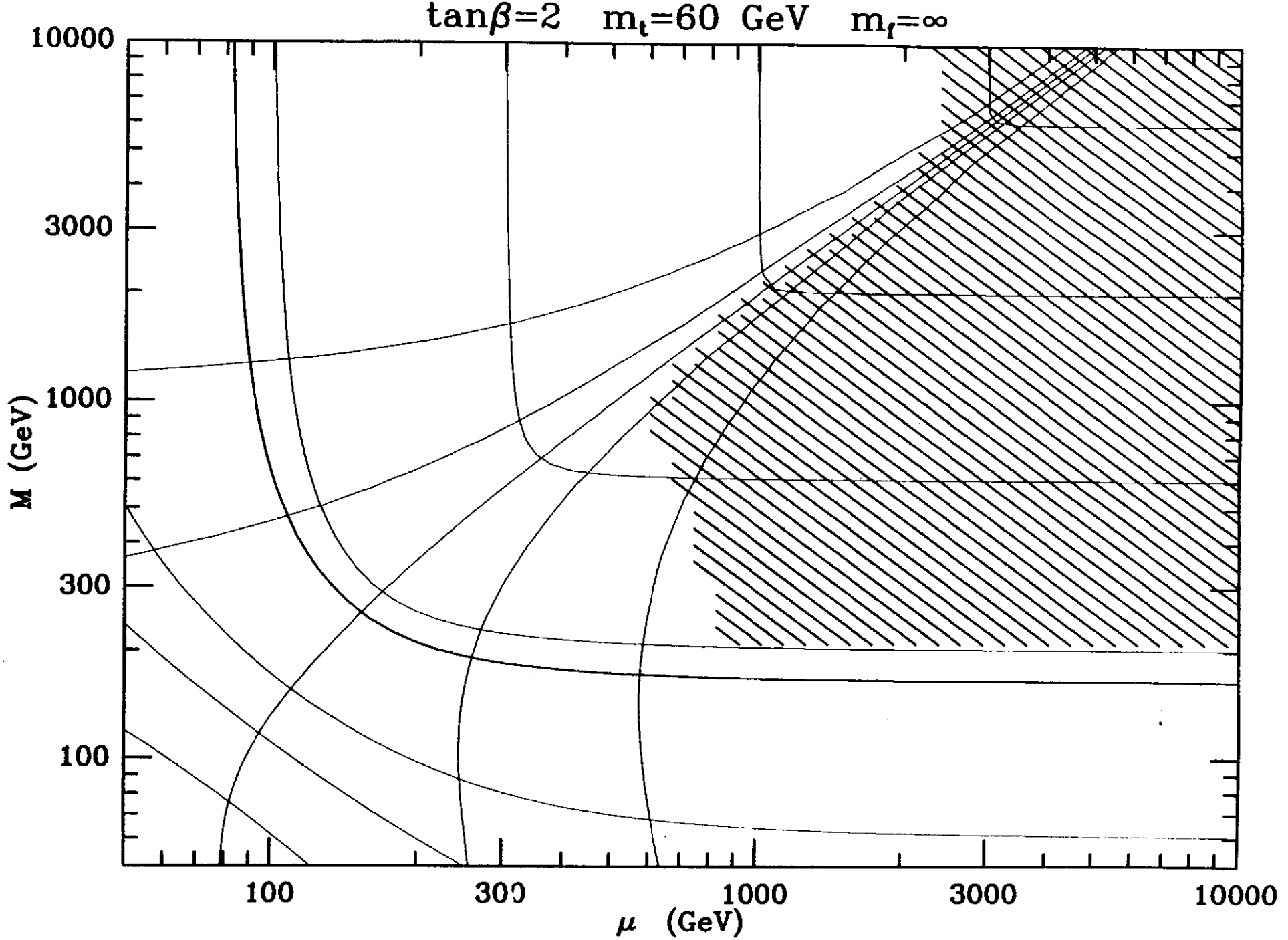
tanβ=2 m_t=60 GeV m_f=∞
10000
3000
1000
300
100
M (GeV)
100
300
1000
3000
10000
μ (GeV)

Fig. 13

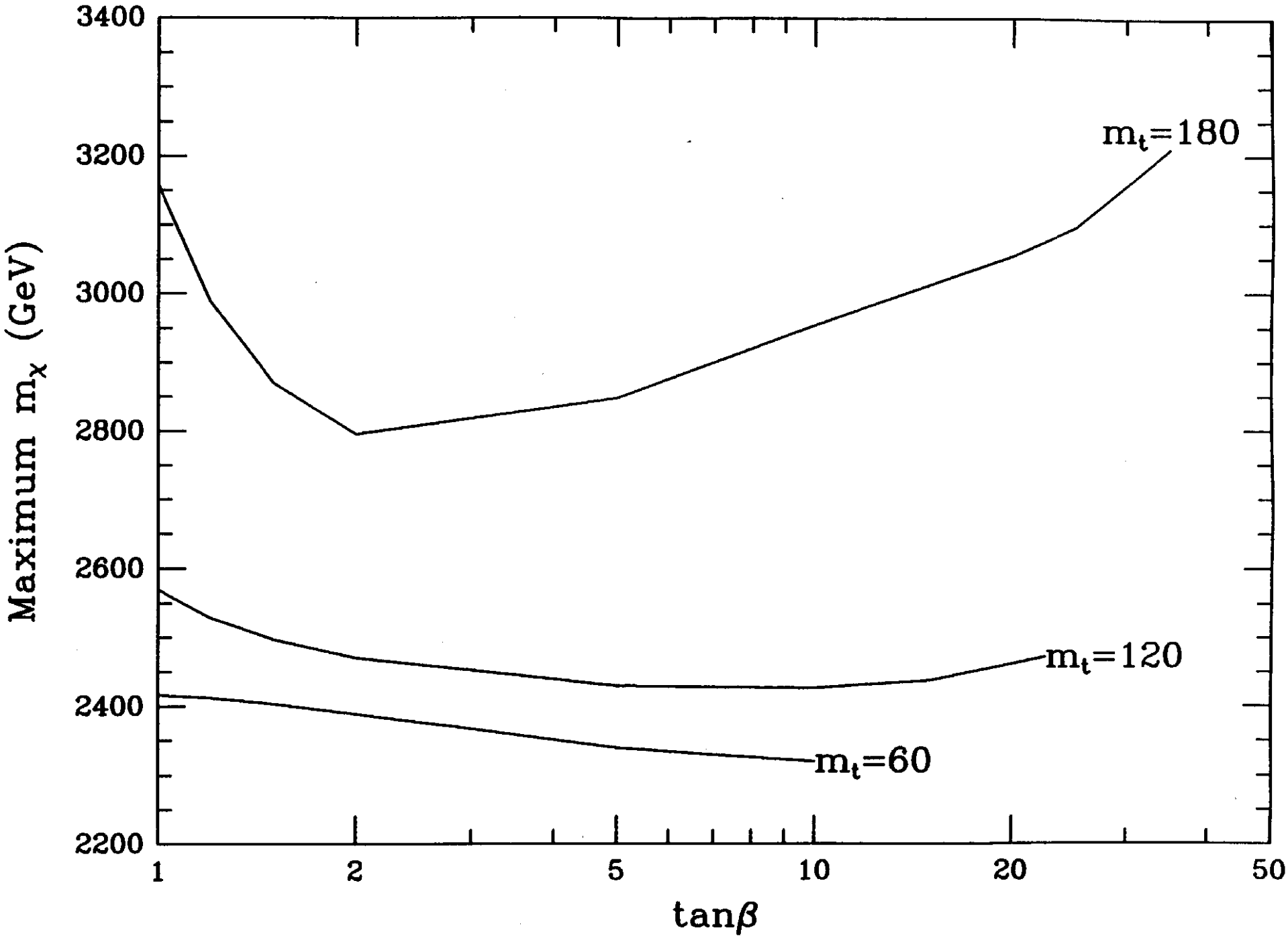
3400
3200
3000
2800
2600
2400
2200
Maximum m_χ (GeV)
m_t=180
m_t=120
m_t=60
1
2
5
10
20
50
tanβ

Fig. 14

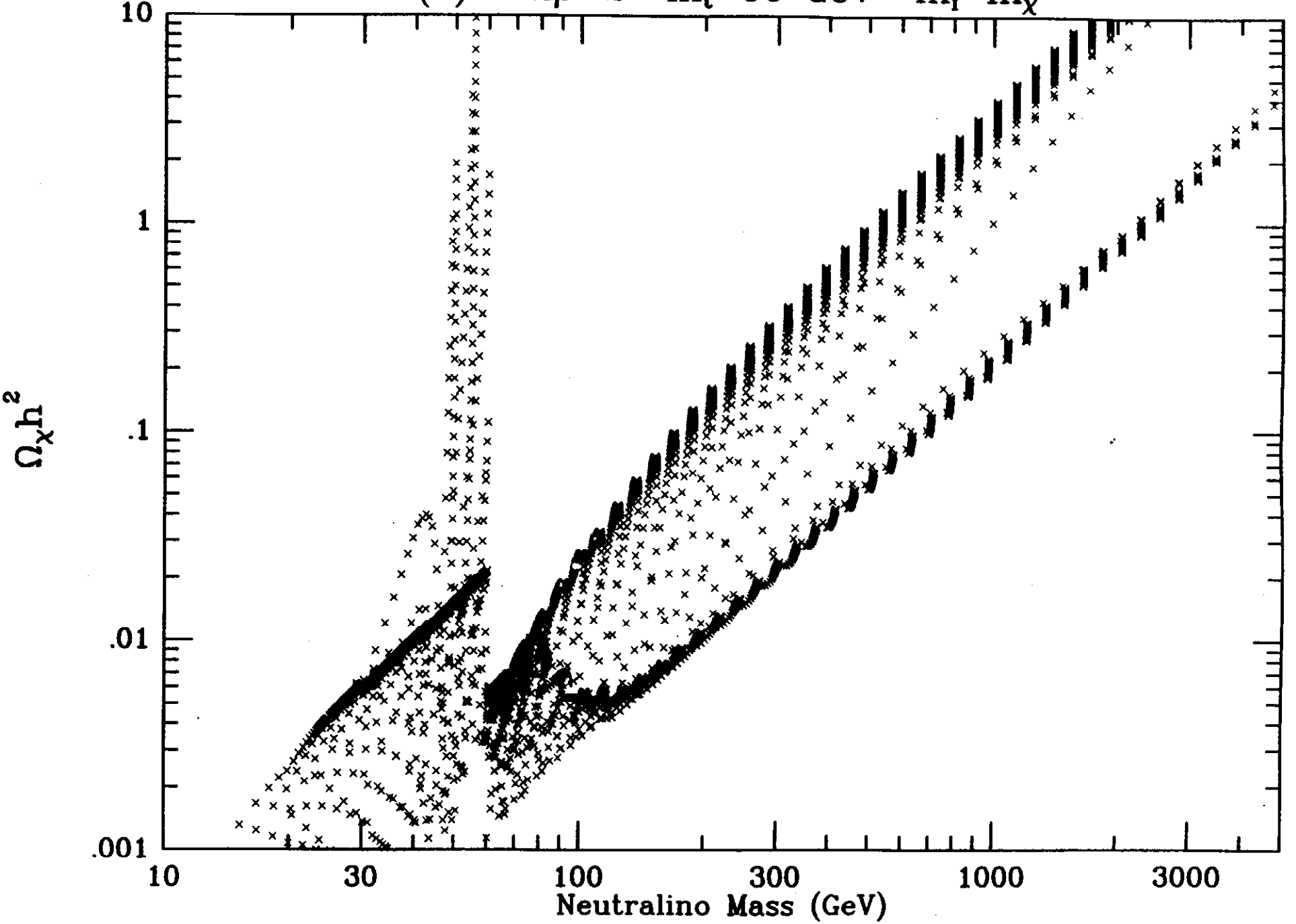
(a) tanβ=2 m_t=60 GeV m_f=m_χ
10
1
.1
.01
.001
$\Omega_\chi h^2$
10
30
100
300
1000
3000
Neutralino Mass (GeV)

Fig. 15(a)

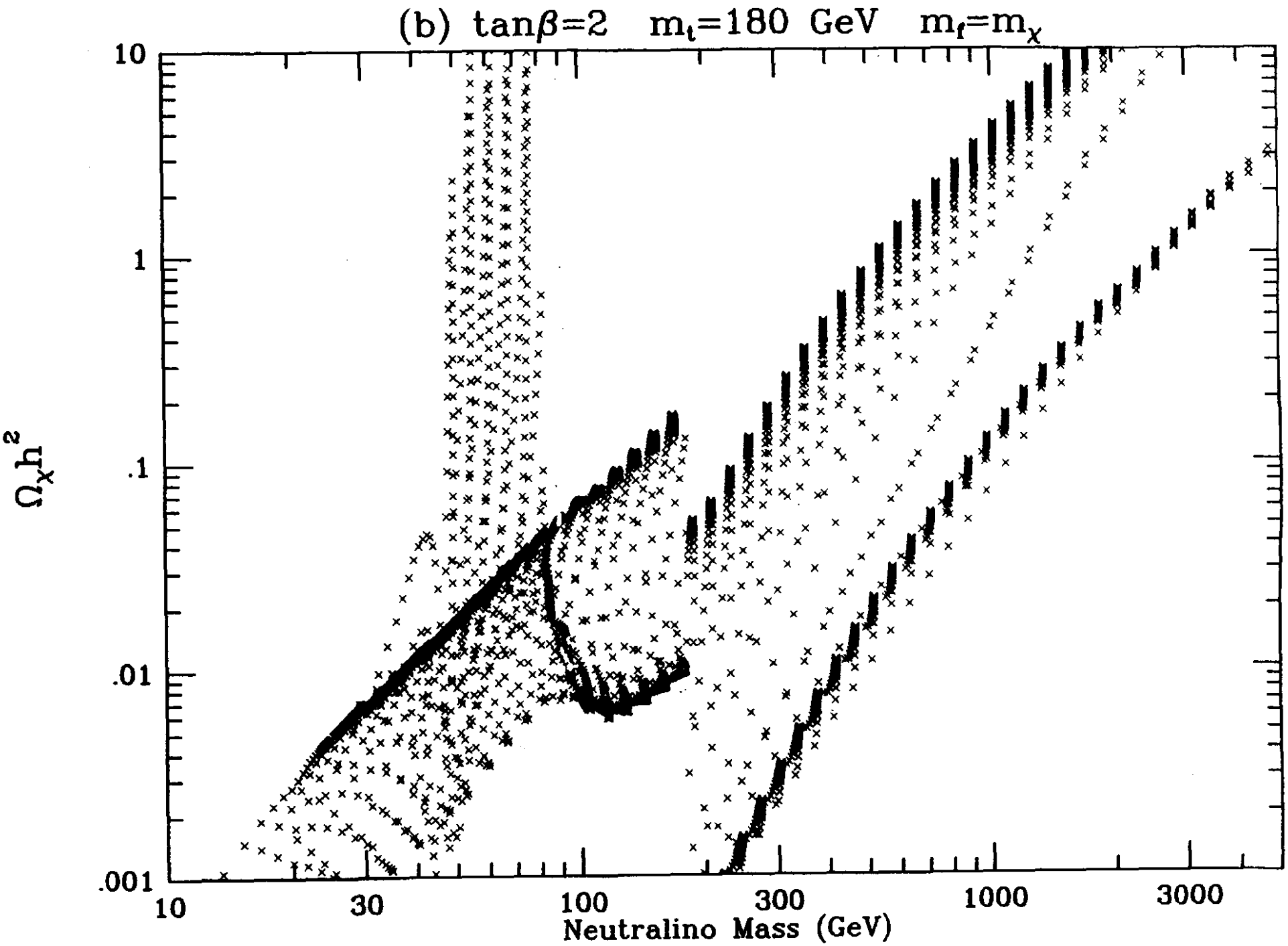
(b) tanβ=2 m_t=180 GeV m_f=m_χ
10
1
.1
.01
.001
$\Omega_\chi h^2$
10
30
100
300
1000
3000
Neutralino Mass (GeV)

Fig. 15(b)

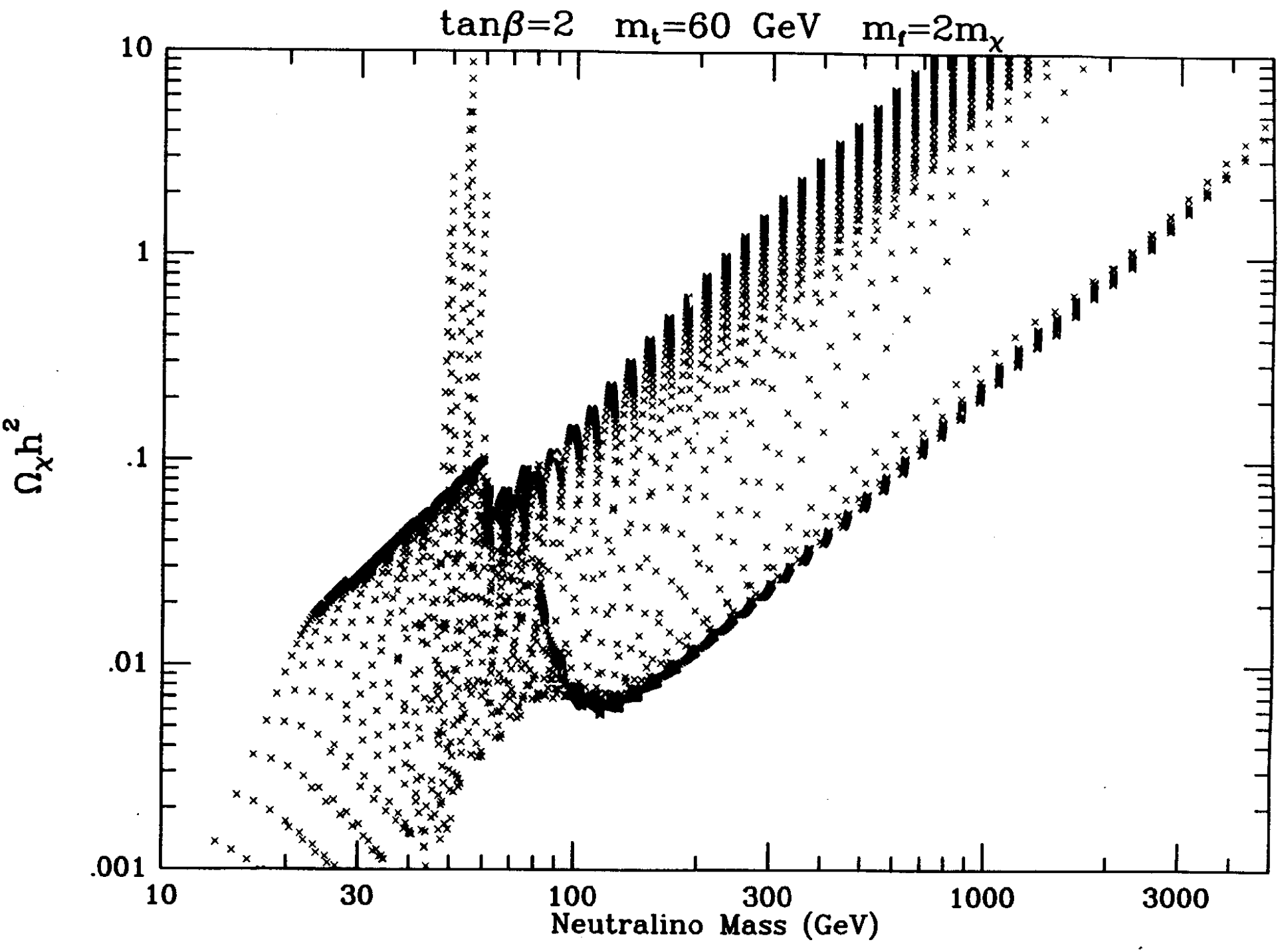
tanβ=2 m_t=60 GeV m_f=2m_χ
10
1
.1
.01
.001
Ω_χh^2
10
30
100
300
1000
3000
Neutralino Mass (GeV)

Fig. 16

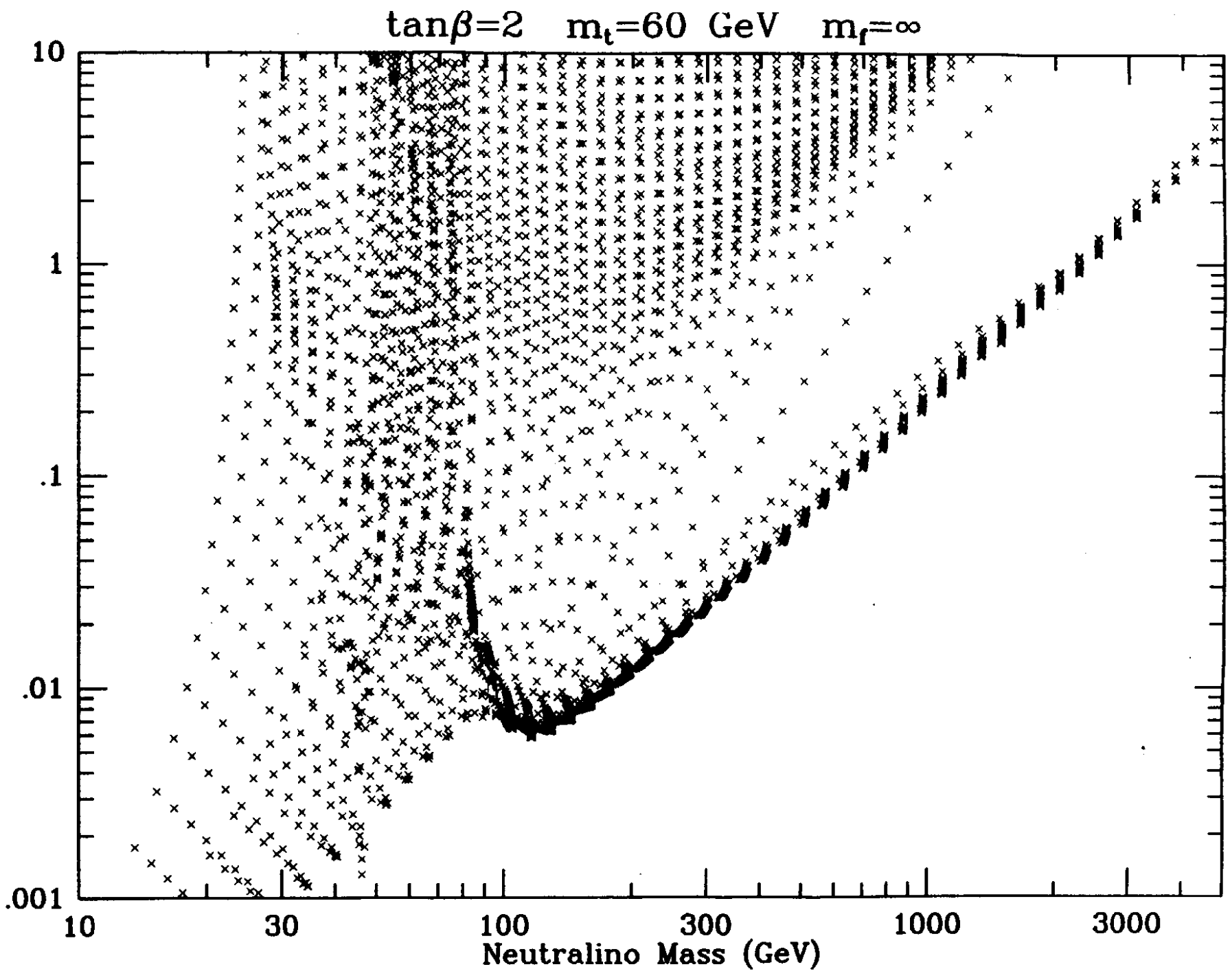
tanβ=2 m_t=60 GeV m_f=∞
10
1
.1
.01
.001
Ω_χh^2
10
30
100
300
1000
3000
Neutralino Mass (GeV)

Fig. 17

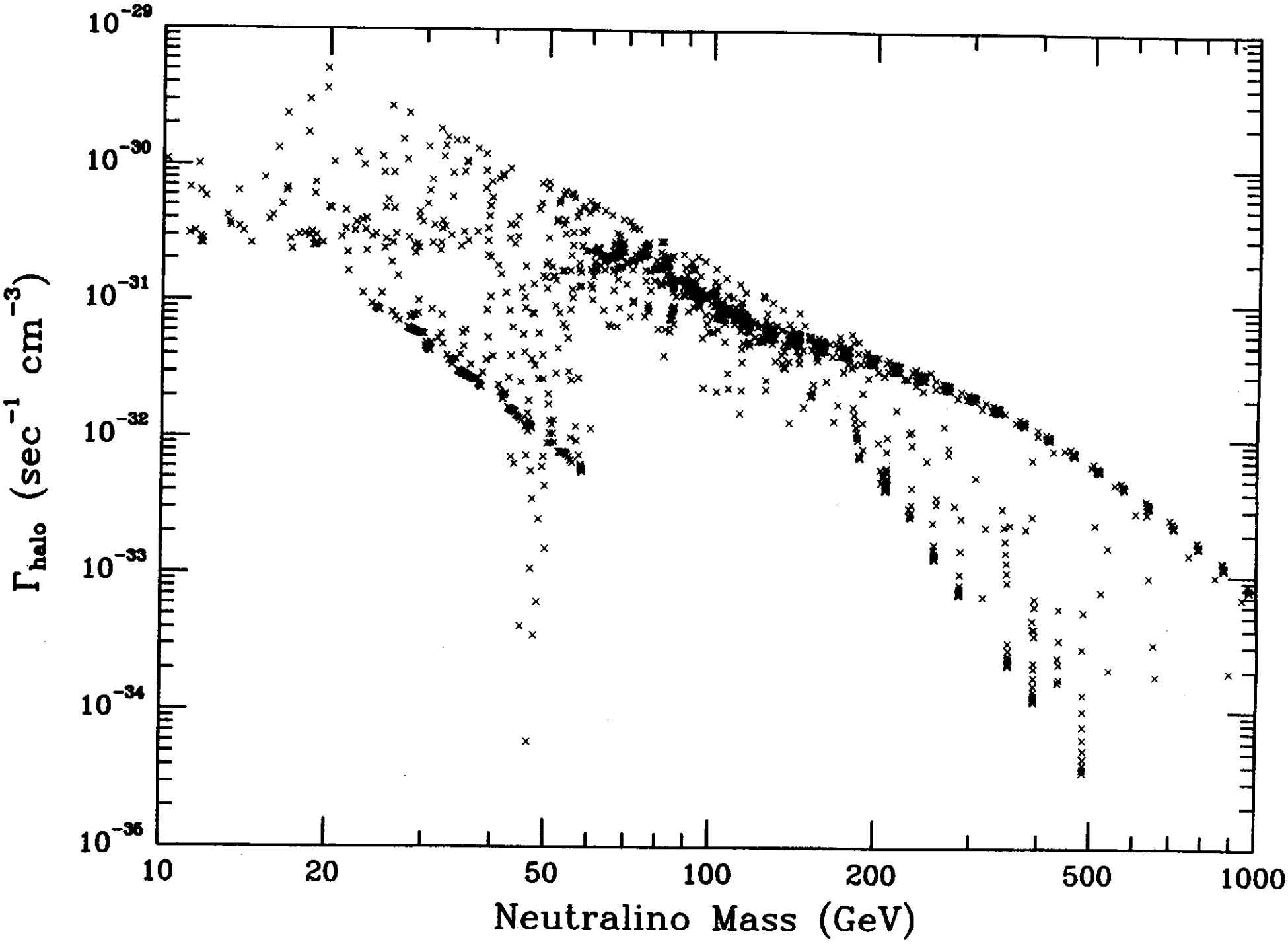
10^{-29}
10^{-30}
10^{-31}
10^{-32}
10^{-33}
10^{-34}
10^{-35}
Γ_{halo} (sec^{-1} cm^{-3})
10
20
50
100
200
500
1000
Neutralino Mass (GeV)

Fig. 18